Title

Nitrogen Fate and Transport in a Conventional Onsite Wastewater Treatment System Installed in a Clay Soil: A Nitrogen Chain Model

Journal

Vadose Zone Journal, 12(3)

ISSN

1539-1663

Authors

Bradshaw, James K
Radcliffe, David E
Šimůnek, Jiří
et al.

Publication Date

2013-08-01

DOI

10.2136/vzj2012.0150

Peer reviewed

Original Research

James K. Bradshaw*
David E. Radcliffe
Jiří Šimůnek
Assaf Wunsch
John E. McCray

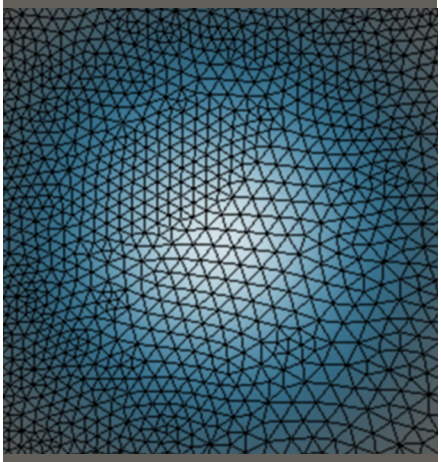

Nitrogen cycling in clay-textured soils with onsite wastewater treatment systems is studied and modeled much less often than sand- and loam-textured soils because there is little data on onsite wastewater treatment system performance in these soils. An N chain model with water-content dependent first-order transformation rates for nitrification and denitrification was developed and calibrated using data from a conventional onsite wastewater treatment system installed in a clay-textured soil. The model predicted the N removal in the system. Estimates of N loss were specific to clay-textured soils and should be valuable to TMDL developers who need to predict load allocations for non-point sources in the Piedmont.

J.K. Bradshaw and D.E. Radcliffe, 3111 Miller Plant Sciences Bldg., Crop and Soil Sciences Dep., Univ. of Georgia, Athens, GA 30602; J. Šimůnek, Dep. of Environmental Sciences, Univ. of California Riverside, Riverside, CA 92521; A. Wunsch and J.E. McCray, Dep. of Civil and Environmental Engineering, Hydrologic Science and Engineering Program, Colorado School of Mines, Golden, GO 80401. . *Corresponding author (jbradsha@uga.edu).

Vadose Zone J.
doi:10.2136/vzj2012.0150
Received 3 Oct. 2012.

Nitrogen Fate and Transport in a Conventional Onsite Wastewater Treatment System Installed in a Clay Soil: A Nitrogen Chain Model

Nitrogen cycling in clay-textured soils with onsite wastewater treatment systems (OWTS) is studied and modeled much less often than sand- and loam-textured soils because there is little data on OWTS performance in these soils. Information on the nitrogen loads from these systems is needed for quantification of total maximum daily loads (TMDLs). The objective of this study was to calibrate a 2D HYDRUS model using experimental soil pressure head and vadose zone nitrogen (N) and chloride (Cl) data from a conventional OWTS that was installed in a clay soil in the Piedmont region of Georgia. An N chain model with water-content dependent first-order transformation rates for nitrification and denitrification was developed. The overall predicted soil pressure heads and solute concentrations were similar to data collected from the field experiment. The calibrated model made it possible to estimate water and solute fluxes in the drainfield and N losses from the OWTS. The estimated annual N loss from leaching at the lower boundary of the experimental drainfield was 3.8 kg yr^{-1}. Scaled up to an OWTS size typical for GA and a zoning density of 5 homes ha^{-1}, the N load to groundwater would be 57.4 kg ha^{-1} yr^{-1}, which is comparable to agricultural production losses to groundwater. The model predicted 52% of the N removal in the system was from denitrification, whereas plant uptake and change in N storage accounted for $\leq$5% of the N loss. These estimates were specific to clay-textured soils and should be valuable to TMDL developers who need to predict load allocations for nonpoint sources in the Piedmont.

Abbreviations: DS, downslope; OWTS, onsite wastewater treatment system; RMSE, root mean squared error; STE, septic tank effluent; TDR, time domain reflectometry; TEMP, temperature; TKN, total Kjeldahl nitrogen; TMDL, total maximum daily load; U, under trench bottoms; WC, water content.

Most nutrient total maximum daily loads in watersheds that include suburban areas attribute part of the nonpoint source N load to OWTSs (USEPA, 2010; GADNR, 2009; NCDENR, 2001). However, the exact contribution from these systems is unknown because the extent to which denitrification reduces the load has not been documented. In a review of the literature on modeling of OWTSs, McCray et al. (2009) concluded that the biggest question in modeling N in OWTSs was under what conditions and to what extent does denitrification occur. Recent literature reviews on OWTSs and soil properties indicated that clay textured soils are studied much less than sand and loam textured soils (McCray et al., 2009; Twarakavi et al., 2010). OWTSs are typically installed in clay soils in the Piedmont region of the southeastern United States and an understanding of their hydraulic and treatment capabilities is necessary.

Nitrogen cycling in the drainfield of OWTSs is a dynamic process. Many factors are involved that affect the type of N compounds present in the system. These factors include the initial N compound, number, and types of microbes present, oxygen concentration and diffusion rate, carbon concentration, pH, temperature, and surface charge of soil particles. Of these factors, oxygen concentration and diffusion rates in the drainfield may be the most important. Soil moisture content, which is relatively easy to measure, is often used as a surrogate for combined oxygen concentration and diffusion rates. In addition, OWTS drainfields commonly cycle between saturated and unsaturated conditions over short time periods because they are time-dosed or because of intermittent water use by the homeowners (e.g., showering in the morning or washing dishes in the evening). During wetting and drying cycles, soil moisture conditions fluctuate in the range near saturation where N mineralization, nitrification, and denitrification are all possible.

N cycling at the drainfield scale is not easily measured because of the complex interactions that take place during wetting and drying cycles. Water flow in soils is three-dimensional and analytical solutions for multidimensional water flow in soils are limited over spatial and temporal scales. However, numerical solutions of multidimensional water flow problems using computer simulation models can improve our understanding of OWTSs and help to quantify processes that are not easily measured. An example is the HYDRUS model developed by Šimůnek et al. (2008). The HYDRUS model is a finite element numerical model capable of simulating water flow, solute transport, and heat flow in soil in one, two, and three dimensions.

Several researchers have used HYDRUS (1D, 2D, and 3D) to model water movement in OWTS. Radcliffe and West (2009) simulated trench hydraulics with HYDRUS and developed a spreadsheet tool to estimate design hydraulic loading rates in different soils. Bumgarner and McCray (2007) used HYDRUS-1D to estimate the unsaturated hydraulic conductivity parameters in the van Genuchten (1980) equation for OWTS biomats and concluded that higher hydraulic loading rates were related to greater reductions in the hydraulic conductivity of the biomat. Radcliffe et al. (2005) compared infiltration rates between gravel and chamber systems and concluded that gravel systems had reduced infiltration rates but the differences between systems were less than claimed by the chamber system manufacturers.

HYDRUS (2D and 3D) has also been used to model fate and transport of septic tank effluent (STE) contaminants in OWTSs. Beggs et al. (2004) modeled the nitrification–denitrification chain reaction to predict the effect of low and high dosing rates on N leaching from a subsurface drip system installed in loam, sandy loam, and clay loam textured soils and reported N removal from denitrification ranged from 20 to 60%. They concluded that N treatment (i.e., denitrification) was enhanced by long residence times in the soil. Hassan et al. (2008) simulated effluent movement and N transport through a subsurface drip system installed in a sandy loam soil and concluded that strong correlations between measured and simulated soil water potentials and N concentrations indicated that HYDRUS was an effective tool for evaluating OWTSs. Pang et al. (2006) simulated clustered OWTS installed in silt loam and sandy loam textured soils to determine their impact on groundwater quality in New Zealand and concluded that clustered OWTSs had a cumulative impact on NO_3–N concentration in groundwater.

Beggs et al. (2011) modeled the fate of N in subsurface drip systems using a HYDRUS model that included water content dependence and temperature dependence functions for solute transport reactions. Nitrification first-order rate coefficients increased linearly at volumetric water contents between 0.10–0.15 $cm^3\ cm^{-3}$ and decreased linearly at volumetric water contents between 0.26 and 0.45 $cm^3\ cm^{-3}$ depending on soil texture. The nitrification rate was optimal at water contents between 0.15 and 0.26 $cm^3\ cm^{-3}$. Denitrification rate coefficients decreased linearly from saturated water content (e.g., water contents between 0.40–0.45 $cm^3\ cm^{-3}$) to a threshold water content between 0.22 and 0.27 $cm^3\ cm^{-3}$ depending on soil texture. The thermal activation energies were 64,000 and 54,000 J mol^{-1} N for nitrification and denitrification, respectively. The authors applied their model to a clay loam textured soil and concluded that soil moisture contents that fluctuated between field capacity and near-saturated conditions may provide the best overall conditions for N removal. Their model results indicated that modeling nitrification and denitrification as a function of water content produced reasonable results. The N losses ranged from 30 to 70% for generic soil types (e.g., sandy loam, loamy sand, and silt loam). They suggested N losses of 50% could be expected in finer textured soils (e.g., clay loam) because denitrification may be enhanced by long retention times in the soil.

The objective of this study was to fit a HYDRUS model using soil pressure head and vadose zone N and Cl data from a conventional (i.e., gravel fill) OWTS that was installed in a clay soil in the Piedmont region of Georgia (Bradshaw and Radcliffe, 2013, this issue). The conventional OWTS consisted of a septic tank and three trenches filled with washed gravel (1.3–5.1 cm diameter). The model was used to estimate annual N losses to groundwater from the drainfield. Water content and temperature dependent solute fate and transport were considered in the model.

Materials and Methods

We used HYDRUS version 2.01 to model water flow and solute transport in variably saturated soil. The HYDRUS model is a finite-element model that uses a numerical solution to the Richards (1931) equation to simulate variably saturated water flow in soil. There are several equations in the model for describing the soil water retention and unsaturated hydraulic conductivity functions. We used the van Genuchten (1980) equation for the water retention curve:

$$\theta(h)=\frac{\theta_s-\theta_r}{\left[1+(-\alpha h)^n\right]^m}+\theta_r \qquad [1]$$

where α (L^{-1}), m (dimensionless), and n (dimensionless) are fitted parameters, $\theta(h)$ is the volumetric water content ($L^3\ L^{-3}$), θ_s is the saturated volumetric water content ($L^3\ L^{-3}$), and θ_r is the residual volumetric water content ($L^3\ L^{-3}$). We also used the unsaturated hydraulic conductivity function $K(h)$ (LT^{-1}) from van Genuchten (1980):

$$K(h)=K_s\left|\frac{\theta(h)-\theta_r}{\theta_s-\theta_r}\right|^{0.5}\left(1-\left\{1-\left|\frac{\theta(h)-\theta_r}{\theta_s-\theta_r}\right|^{1/m}\right\}^m\right) \qquad [2]$$

where K_s is the saturated hydraulic conductivity (L T^{-1}), m is the fitted parameter from Eq. [1], and it is assumed that $m = 1 - 1/n$.

Initial estimates of the water retention parameters for Eq. [1]–[2] were predicted with soil water retention data and the RETC computer code (van Genuchten et al., 1991). Soil water retention curves for the A horizon were constructed from volumetric water content measurements using intact cores (8.9 cm diameter by 6.0 cm long) that were assembled into pressure cells (Soil Moisture Equipment Corp., Santa Barbara, CA). Soil water retention parameters for the Bt and BC horizons were determined from the measured average time-domain reflectometry (TDR) water contents and tensiometer pressure heads at 15 cm under (U) and 15 cm downslope (DS) positions. These data covered a narrow range of pressure heads near saturation but this was the range of the field experiment being modeled. The K_s values were measured in the field with compact constant head permeameters (K_{sat} Inc., Raleigh, NC).

Solute transport in HYDRUS is described by a numerical solution to the advection-dispersion equation (ADE). When linear adsorption and chemical equilibrium (no kinetics of adsorption) are assumed, the ADE is:

$$\frac{\partial \theta c}{\partial t} + \rho_b K_d \frac{\partial c}{\partial t} = \frac{\partial}{\partial x}\left[\theta D_e \frac{\partial c}{\partial x}\right] + \frac{\partial}{\partial z}\left[\theta D_e \frac{\partial c}{\partial z}\right] - \frac{\partial J_{wx} c}{\partial x} - \frac{\partial J_{wz} c}{\partial z} - \theta \mu c - Sc \quad [3]$$

where θ is the volumetric water content (L^3 L^{-3}), c is the dissolved concentration of a solute (M L^{-3}), t is time (T), K_d is an adsorption coefficient (L^3 M^{-1}), D_e is the effective dispersion coefficient tensor (L^2 T^{-1}), z is the vertical dimension (L), x is the horizontal dimension (L), J_{wz} is the Darcy water flux (L T^{-1}) in the vertical direction, J_{wx} is the Darcy water flux (L T^{-1}) in the horizontal direction, μ is the first-order rate constant for solute transformation processes (T^{-1}) and S is root uptake rate (T^{-1}).

The model space was designed based on a scaled down OWTS installed in Griffin, GA (Bradshaw and Radcliffe, 2013, this issue). Briefly, the field experiment consisted of a septic tank connected to a drainfield with three 10-m long by 1-m wide trenches that were 2.5 m apart from center-to-center. The Cecil soil (*cecil fine kaolinitic thermic typic kanhapudult*) in Griffin consisted of a thin surface layer (A horizon) underlain by a thick subsurface layer (Bt horizon) that transitioned to a soil-saprolite mixture starting at 1.5 m below the soil surface (BC horizon). The trenches were filled with gravel and contained a perforated pipe to distribute wastewater into the drainfield. The drainfield and trench were modeled in HYDRUS as a cross section with one axis vertical and the other horizontal (Fig. 1). One half of the drainfield was used for the model space assuming the middle of the trench was an axis of symmetry and formed a no-flux boundary on the left side of the model space, except for the perforated pipe which was a variable flux boundary. The model space was 125 cm in the horizontal dimension. This placed the right boundary approximately at the midpoint between two trenches, and assumed trenches were centered at 2.5 m (i.e., typical spacing for a conventional OWTS in Georgia and the spacing in our field experiment). The model space was 162 cm in the vertical direction (the depth of our deepest suction lysimeter) with the trench bottom placed at 72 cm below the soil surface. The soil surface formed the top of the model space and was treated as an atmospheric boundary (infiltration and evaporation). The simulated trench was 45 cm in width (i.e., half that of a full trench width) and 30 cm in height. The boundary condition at the bottom of the model space represented a deep water table with a vertical pressure head gradient equal to zero (i.e., $dh/dz = 0$), which required only gravity to cause vertical flow.

The model space consisted of five materials that represented the three soil horizons, the gravel, and a 2-cm thick biomat at the trench-soil-interface on the bottom and sidewall (Fig. 2). The model space also contained eight observation nodes placed in the drainfield below the depth of the trench bottoms. Four observation nodes were placed in the U position at 15, 30, 60, and 90 cm and four observation nodes were placed DS of the trench at the same depths. The observation nodes in the model space represented tensiometers and lysimeters that were installed at the Griffin site. Tensiometers and lysimeters were installed in each trench at 3.3 m and 6.6 m from the trench inlet. The tensiometers were located at the 15 cm U and 15 cm DS positions and the lysimeters were located at the 15-, 30-, 60-, and 90-cm U and DS positions.

There are two options for modeling root water uptake in HYDRUS. We chose the Feddes et al. (1978) model for actual plant uptake of water, $S(h)$ (T^{-1}):

$$S(h) = \alpha(h) S_p \quad [4]$$

where $\alpha(h)$ is a dimensionless stress function of soil pressure head that varies between zero and one, and S_p is the potential water uptake rate (T^{-1}). In this model, the stress function is zero at a pressure head close to saturation (h_1) and increases linearly to one as pressure heads decrease. The stress function is one over an optimum pressure head range (h_2 to h_3) and then decreases linearly to zero at permanent wilting point (h_4). The breakpoint pressure heads were taken from the HYDRUS database for grass ($h_1 = -10$ cm, $h_2 = -25$ cm, $h_3 = -200$ to -800 cm depending on the transpiration rate, and $h_4 = -8000$ cm). We assumed a relative root distribution that was maximal between 0 and 5 cm and then decreased linearly to a depth of 100 cm. The field experiment OWTS was installed in a tall fescue (*S. phoenix*) grass cover and the root distribution was modeled based on the root mass distributions for tall fescue described by Crush et al. (2005). Roots were excluded from trench space. No plant uptake preference for the

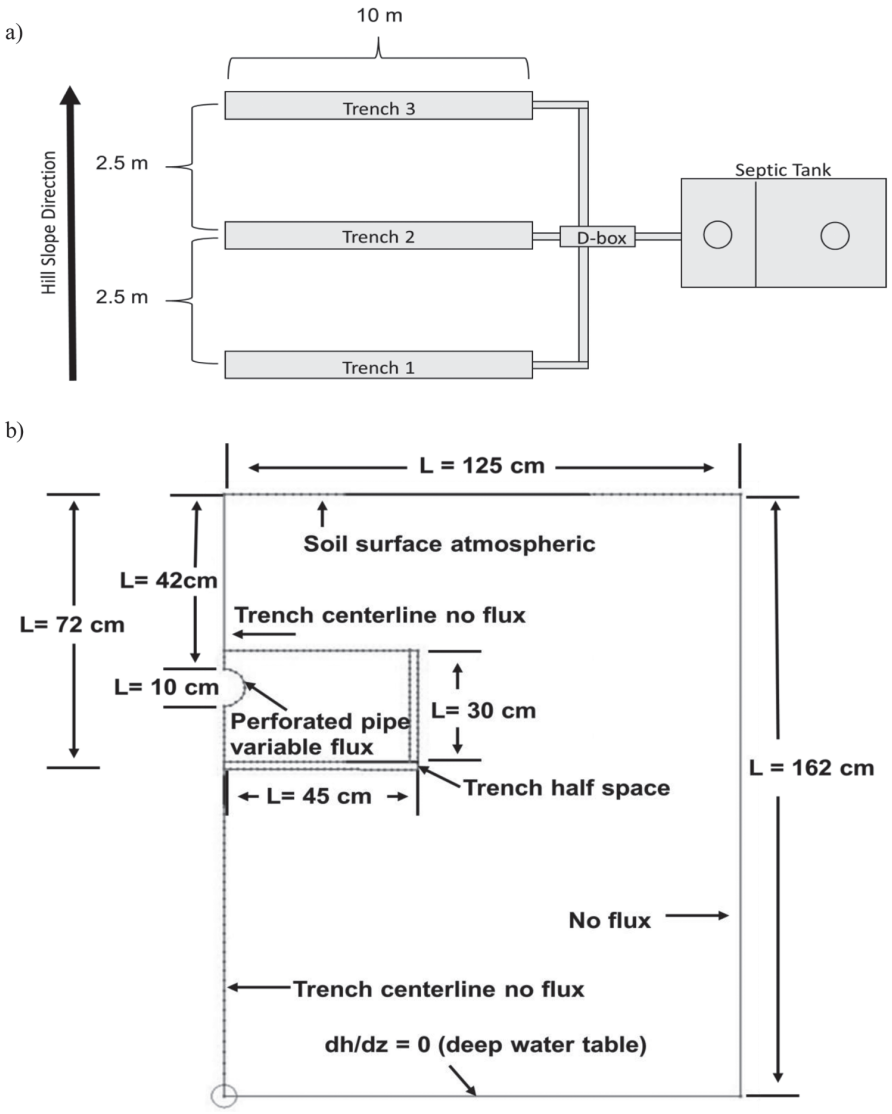

Fig. 1. Simple plan view of experimental onsite wastewater treatment system (OWTS) (a). Model dimensions and boundary conditions for the HYDRUS simulations (b). Dimensions for length (L) are in cm.

form of nitrogen was included in the model. This assumption is consistent with data reported in a study by Schrader et al. (1972), who showed that plant uptake rates were similar when NH_4–N and NO_3–N were both present.

The initial condition for soil pressure head was set to −50 cm for the entire model space. We started with a relatively wet profile to minimize the time it would take to reach the prevailing moisture conditions during the experiment. The initial condition for concentrations of NH_4^+, NO_3^-, and Cl^- were set to 0 mg L^{-1} to allow those concentrations to build over time as the OWTS matured. The Griffin OWTS was new and the model was designed to capture the development of the drainfield. The atmospheric boundary condition in HYDRUS is a time-variable boundary condition appropriate for the soil surface that required measurements of precipitation and evapotranspiration (Fig. 1). Precipitation was recorded daily at the Griffin OWTS and the data was included in the atmospheric boundary condition (Bradshaw and Radcliffe, 2013, in this issue). Potential evapotranspiration was measured at a weather station located 0.5 km from the Griffin OWTS and was also included in the atmospheric boundary condition (Bradshaw and Radcliffe, 2013, in this issue).

Dosed wastewater inputs at the perforated pipe were simulated with a variable flux boundary condition and we assumed uniform infiltration over the 10-m trench. The dosing rate used at the Griffin OWTS was 2.1 cm d^{-1} dosed every 8 h. Concentrations of total Kjeldahl nitrogen (TKN), NH_4^+, NO_3^-, and Cl^- in the STE were measured once per month at the OWTS. Approximately 75% of the wastewater TKN concentration was NH_4^+ and

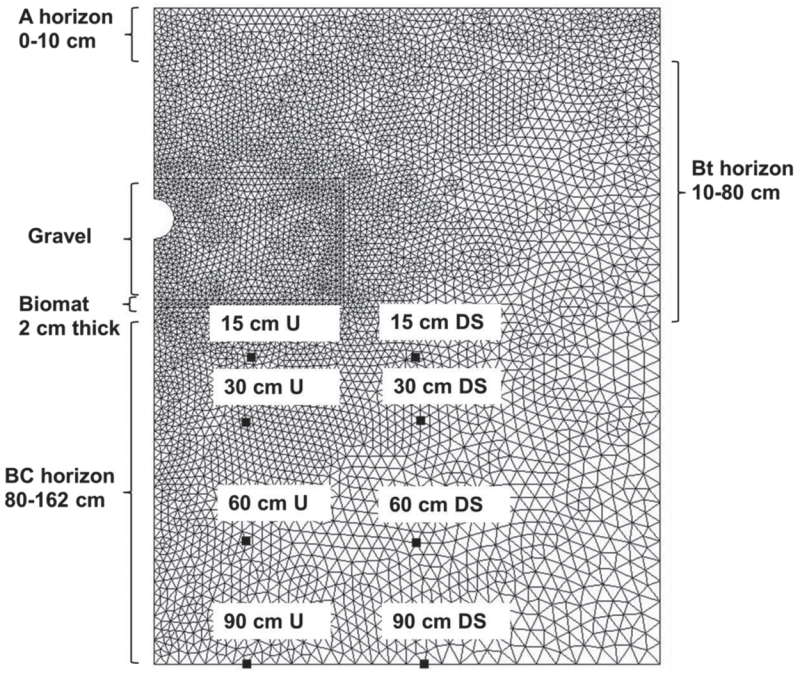

Fig. 2. Model space showing material distribution, and location of observation nodes. The trench was constructed entirely in the Bt horizon. The trench bottom was located above the BC horizon.

NO_3^- concentrations were negligible (Bradshaw and Radcliffe, 2013, in this issue). To account for the total N added to the system, the measured monthly TKN concentrations were used as the N input and we assumed that all of the organic N in the wastewater was converted to NH_4^+ in the trench. The input concentration for NO_3^- was zero. The measured STE concentration varied from month-to-month so the input concentrations for TKN and Cl^- changed on a monthly interval in the variable boundary conditions (i.e., the solute concentration for a particular month was constant over a 1-mo interval and changed for the next month based on the measured concentration in the STE).

A total of 5515 nodes were used in the model space, with the densest network in and around the trench where wastewater entered from the perforated pipe, the biomat zone, and near the soil surface where precipitation and evapotranspiration took place (Fig. 2). The minimum mesh size was 1.5 cm, based on the longest dimension between nodes. The smallest elements were located near the trench bottom and sidewall (Fig. 2). The maximum mesh size was 5.3 cm and was located near the bottom right-hand corner of the model space. The number and distribution of nodes was chosen through a process of trial and error to find the combination that resulted in a numerical solution that converged and maintained a water balance error <1% at all time intervals. The tolerances for iteration convergence were set at a water content of 0.001 $cm^3\ cm^{-3}$ and a pressure head of 1 cm.

The simulation period for the model was from 1 Apr. 2009 to 10 Apr. 2011 (740 d or 17,760 h). The HYDRUS model includes an inverse solution algorithm to fit experimental data. However, the inverse solution method was not used in our model because of very long run times to reach a solution and difficulty in constraining the hydraulic parameter solutions so they would not cause the simulation to crash. Therefore, the model was calibrated in three steps. First, we manually calibrated the model to the tensiometer data measured at the Griffin OWTS over the 17,760 h period. The model was allowed to run through the 17,760 h period and the pressure head output at the 15-cm U and 15-cm DS observation nodes were compared to the drainfield average of the soil pressure heads measured at the respective depths. It was assumed that the biomat had the same soil water retention parameters as the Bt and BC horizons. For the gravel layer, soil water retention parameters were chosen based on the bulk density (for θ_s) and to provide the steepest soil characteristic curve (large value for n) that would not cause the simulation to crash. The gravel K_s was set to an estimate based on falling head measurements in the lab. The values for K_s in each soil horizon were adjusted and the model rerun to find the best fit between the predicted and measured pressure heads over the simulation period based on the root mean squared error (RMSE). The equation for RMSE was:

$$\mathrm{RMSE} = \sqrt{\frac{\sum_{i=1}^{n}\left(\hat{y}_i - y_i\right)^2}{n}} \qquad [5]$$

where $\hat{y}_i$ is the predicted value, y_i is the observed value, and n is the number of observations.

In the second step, we compared predicted and measured concentrations of Cl^- at the 15-, 30-, 60-, and 90-cm U and DS positions, averaged over the drainfield and calibrated the model by manually adjusting the parameters for Cl^- adsorption (K_d), and longitudinal and transverse dispersivity. We measured soil bulk density (ρ_b) on clods taken from the soil at the Griffin site following standard procedures (USDA, 1996). Soils in the Piedmont region exhibit anion exchange due to pH-dependent charges on iron and aluminum oxide minerals so Cl^- adsorption was included in the model. We assumed that Cl^- sorption was linear but allowed the adsorption coefficient to vary depending on horizon. The initial adsorption coefficients were from Cl^- adsorption isotherms developed using soil samples from the subsoil horizons at the Griffin site (Bradshaw and Radcliffe, 2013, in this issue). The average of the Bt1 and Bt2 K_d values were used for the initial estimate of the Bt horizon in the model space. The model was run through 17,760 h and the solute transport parameters for Cl^- were adjusted to find the best fit between the predicted and observed Cl^- concentrations at each respective depth based on RMSE. Error bars represent the standard error of the mean for each lysimeter location in the average simulations for Cl^-, NH_4^+, and NO_3^- (i.e., 15 cm U is the average and standard error from the lysimeter installed at 15 cm under the trench bottom at 3.3 m and 6.6 m in all three trenches). For wet end simulation and dry end simulation (see below), the mean and standard error were calculated using lysimeters located at the wet or dry end, respectively (i.e., the 15 cm U for the wet end simulation is the average and standard error from the lysimeters installed at 15 cm under the trench bottom at 3.3 m in all three trenches).

In the third step, we compared predicted and measured concentrations of NH_4^+ and NO_3^- at the 15-, 30-, 60-, and 90-cm U and DS positions, averaged over the drainfield. We included the input concentration of TKN in the variable flux boundary condition and used the transverse and longitudinal dispersivity values from step two to simulate transport of NH_4^+ and NO_3^-. We used an N chain model to simulate the transformations of N in the drainfield. In nitrification, NH_4^+ is oxidized to NO_2^- and then to NO_3^-:

$$NH_4^+ + \tfrac{3}{2}O_2 \rightarrow NO_2^- + H_2O + 2H^+ \quad [6]$$

$$NO_2^- + \tfrac{1}{2}O_2 \rightarrow NO_3^- \quad [7]$$

In denitrification, NO_3^- is reduced to N_2:

$$2NO_3^- + \tfrac{1}{6}C_6H_{12}O_6 \rightarrow 2NO_2^- + CO_2 + H_2O \quad [8]$$

$$2NO_2^- + 2H^+ + \tfrac{1}{4}C_6H_{12}O_6 \rightarrow N_2 + \tfrac{5}{2}H_2O + \tfrac{3}{2}CO_2 \quad [9]$$

Although there is an intermediate product, NO_2^-, the conversion from NH_4^+ to NO_3^- and from NO_3^- to N_2 is rapid and the reaction can be simplified to two steps (McCray et al., 2005) which we used in our model:

$$NH_4^+ \rightarrow NO_3^- \quad [10]$$

$$NO_3^- \rightarrow N_2 \quad [11]$$

The first-order reaction rates for the change in NH_4^+ and NO_3^- concentrations that result from the nitrification and denitrification chain reaction are:

$$\frac{\partial[NH_4^+]}{\partial t} = -\lambda[NH_4^+] \quad [12]$$

$$\frac{\partial[NO_3^-]}{\partial t} = \lambda[NH_4^+] - \mu[NO_3^-] \quad [13]$$

where λ and μ are the nitrification and denitrification rate coefficients (T^{-1}), respectively, and t is time (T). These rate coefficients can apply to the liquid and/or solid phase. We assumed that they only applied to the liquid phase. The initial solute transport parameters for λ and μ were selected from a range of nitrification and denitrification rates reported in McCray et al. (2005).

HYDRUS incorporates temperature dependence of reaction rates using a modified form of the Arrhenius equation where the user specifies activation energies for a particular reaction (Šimůnek et al., 2008). Activation energies for nitrification (64,000 J mol^{-1} N) and denitrification (54,000 J mol^{-1} N) were taken from Beggs et al. (2011) and Tchobanoglous et al. (2004). Temperature dependence was not considered for adsorption or soil hydraulic properties.

Version 2.01 of HYDRUS (2D and 3D) incorporates water content dependence of reaction rates using a modified form of the Walker (1974) equation:

$$\omega(\theta) = \omega_r(\theta_r)\min\left[1, \left(\frac{\theta^B}{\theta_r}\right)\right] \quad [14]$$

where ω_r is the rate constant (T^{-1}) at the reference water content θ_r, $\omega(\theta)$ is the rate constant (T^{-1}) at the actual water content, θ, and B is a dimensionless solute-dependent parameter. The reference

water content may be different for different soil layers, and is calculated from the reference pressure head, h_r (L), which is considered to be constant for a particular compound (Šimůnek et al., 2008). The Walker (1974) water content dependency function was not the most representative function for nitrification and denitrification rates in our system because it did not allow us to ramp down nitrification at very low water contents.

Instead, we used a saturation–dependency function that varied between zero and one and allowed for more control of nitrification and denitrification rates at the water contents that we observed in our system. These saturation–dependency functions are similar to those implemented in the agricultural model DRAINMOD-N II (Youssef et al., 2005), and are based on Brevé (1994). The saturation dependency function for nitrification ($f_{sw,nit}$) was:

$$f_{sw,nit} = \begin{cases} f_s + (1-f_s)\left(\dfrac{1-s}{1-s_h}\right)^{e2} & s_h < s \le 1 \\ 1 & s_l \le s \le s_h \\ f_{wp} + (1-f_{wp})\left(\dfrac{s-s_{wp}}{s_l-s_{wp}}\right)^{e3} & s_{wp} \le s < s_l \end{cases} \quad [15]$$

where: f_s is the value at saturation, s is the relative water content, s_h is the maximum relative water content for optimal nitrification, f_{wp} is the value at wilting point, s_l is the minimum relative water content for optimal nitrification, s_{wp} is the relative water content at wilting point, and e_2 and e_3 are exponents. The saturation dependency function for denitrification ($f_{sw,denit}$) was:

$$f_{sw,denit} = \begin{cases} 0 & s < s_{dn} \\ \left(\dfrac{s-s_{dn}}{1-s_{dn}}\right)^{e1} & s \ge s_{dn} \end{cases} \quad [16]$$

where s_{dn} is the minimum relative water content for denitrification and $e1$ is an exponent. The first-order rate coefficients for nitrification and denitrification (λ and μ in Eq. [10]–[13]) were multiplied by the appropriate saturation dependency functions ($f_{sw,nit}$ and $f_{sw,denit}$) in the model.

We assumed that NH_4^+ and NO_3^- sorption was linear and allowed the adsorption coefficients to vary depending on the soil horizon or trench. The initial NH_4^+ adsorption coefficients were estimated from adsorption isotherms constructed using soil samples from the subsoil horizons at the Griffin site (data not shown). The initial adsorption coefficients for Cl^- were used for NO_3^-.

Our field study showed wastewater was not evenly distributed over the drainfield. The 3.3 m end of the trenches (nearest the inlet) tended to be wetter than the 6.6 m end, as indicated by pressure head and trench ponding data. To capture these differences, we modeled nitrogen transport in the contrasting wet and dry ends of the drainfield, as well as the overall drainfield. We used the overall average Cl^- concentration for each end of the trenches as an indicator of how much of the total dose the proximal and distal ends of the trenches received. On average, Cl^- concentrations were 1.6 times higher at 3.3 m than at 6.6 m. Two additional HYDRUS simulations were conducted to model the spatial effect of the drainfield receiving different amounts of effluent. The effluent dose was adjusted so that the 3.3 m and 6.6 m simulations would receive the specified ratio of doses. As such, the N chain model was calibrated using three subsets of solute concentration data measured at the field site: the average concentrations for each depth and position (U and DS) at the 3.3 m distance (wet end simulation), the average concentrations at each depth and position at the 6.6 m distance (dry end simulation), and the overall (i.e., 3.3 m and 6.6 m combined) average concentrations at each depth and position (drainfield average simulation). Simulated NH_4^+ and NO_3^- were compared to NH_4^+ and NO_3^- concentrations measured at the Griffin OWTS. The model was run through 17,760 h and the solute transport parameters for NH_4^+ and NO_3^-, including the water-content dependence parameters, were adjusted to find the best fit between the predicted and observed NH_4^+ and NO_3^-, concentrations.

To estimate N loads to groundwater from a mature OWTS where adsorption of N was assumed to be at steady state, we ran our calibrated drainfield average model for an additional 2 yr using the same weather data set. For this simulation, we imported the initial conditions from the end of the first 2-yr cycle simulations. Fitted parameters were assumed to remain constant for the additional 2-yr cycle, though they may change as a system matures.

Results and Discussion

Drainfield Average Simulations: Pressure Head

Overall, the drainfield average simulated pressure heads at 15 cm U and DS of the trenches were comparable to the average drainfield pressure heads at the Griffin OWTS (Fig. 3) (RMSE = 37.4 and 35.8 cm for 15 cm U and 15 cm DS, respectively). Distinct wet periods and dry periods in both years are apparent, especially in the measured pressure head data at the DS position. The simulated pressure heads were lower than the measured pressure heads at both positions, but the model was able to capture the dynamic fluctuations in pressure head that occurred during rainfall. The key to simulating these fluctuations was the values for α and n parameters in Eq. [1] (Table 1). Using data obtained from a fit of the field TDR water contents and tensiometer pressure heads produced values that caused the water retention curve to change in the range of pressure heads common in the field (between zero and −100 cm). The 15-cm zone directly below the trench bottoms was near saturation ($h \ge 0$ cm) for most of the simulation and it

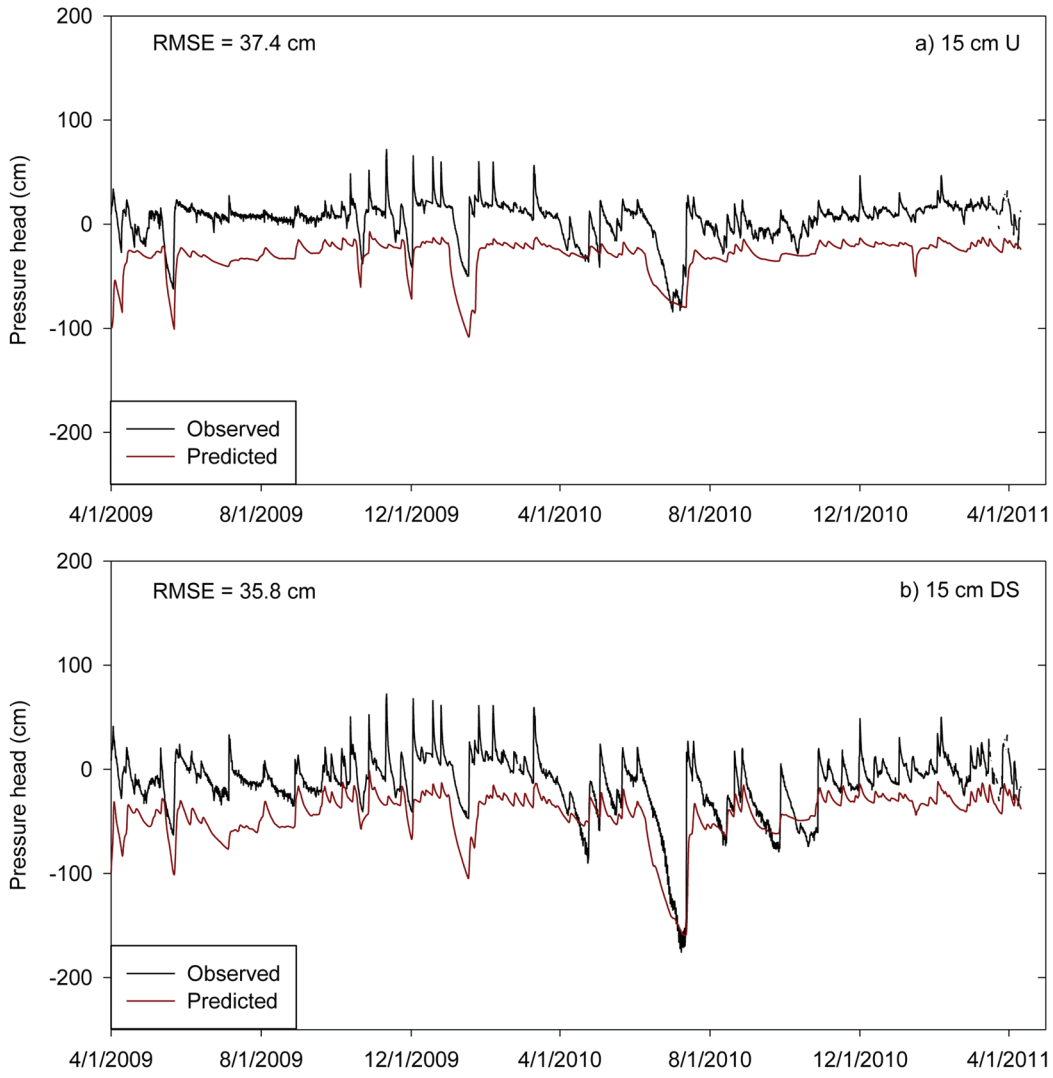

Fig. 3. Drainfield average predicted and observed pressure heads at the 15 cm under tranch bottom (U) (a) and 15 cm downslope (DS) (b) observation nodes.

Table 1. Calibrated HYDRUS water flow parameters.

Material	θ_r	θ_s	α	n	K_s
	—— $cm^3\ cm^{-3}$ ——		cm^{-1}		$cm\ h^{-1}$
A	0.0485	0.3904	0.0347	1.747	15.0
Bt	0.0000	0.3834	0.0084	1.415	0.945
Gravel	0.0100	0.3700	0.3000	3.000	305
BC	0.0000	0.3834	0.0084	1.415	0.145
Biomat	0.0000	0.3834	0.0084	1.415	0.010

was difficult to calibrate the model in that range of pressure heads because the model became unstable near saturation and numerical convergence was not possible. The 15-cm zone downslope from the trench bottoms was also near saturation; however, the pressure heads were lower than at the 15-cm U position (Fig. 3b). The key to simulating lower pressure heads in the DS compared to the U position was inclusion of a biomat with a reduced K_s along the trench bottom and sidewall (Table 1). This caused higher pressure heads in the trench and directly below the trench. This may seem counterintuitive in that we think of biomats causing a larger difference in pressure heads in the trench and below the trench, which they do. However, by raising the pressure head in the trench sharply, they also raise the pressure head below the trench, provided the K_s of the biomat was not too low compared to the soil, which is likely to be the case in a clayey soil (Table 1). The simulated pressure heads in the downslope position were also lower than the measured pressure heads. There were several times over the 17,760 h simulation where the observed pressure heads were very negative (e.g., −150 cm in July 2010). This was due to malfunctions in the dosing apparatus at the Griffin OWTS. When the OWTS did not receive a dose for several days, the soil pressure heads became more negative. We removed or reduced the dose when there were

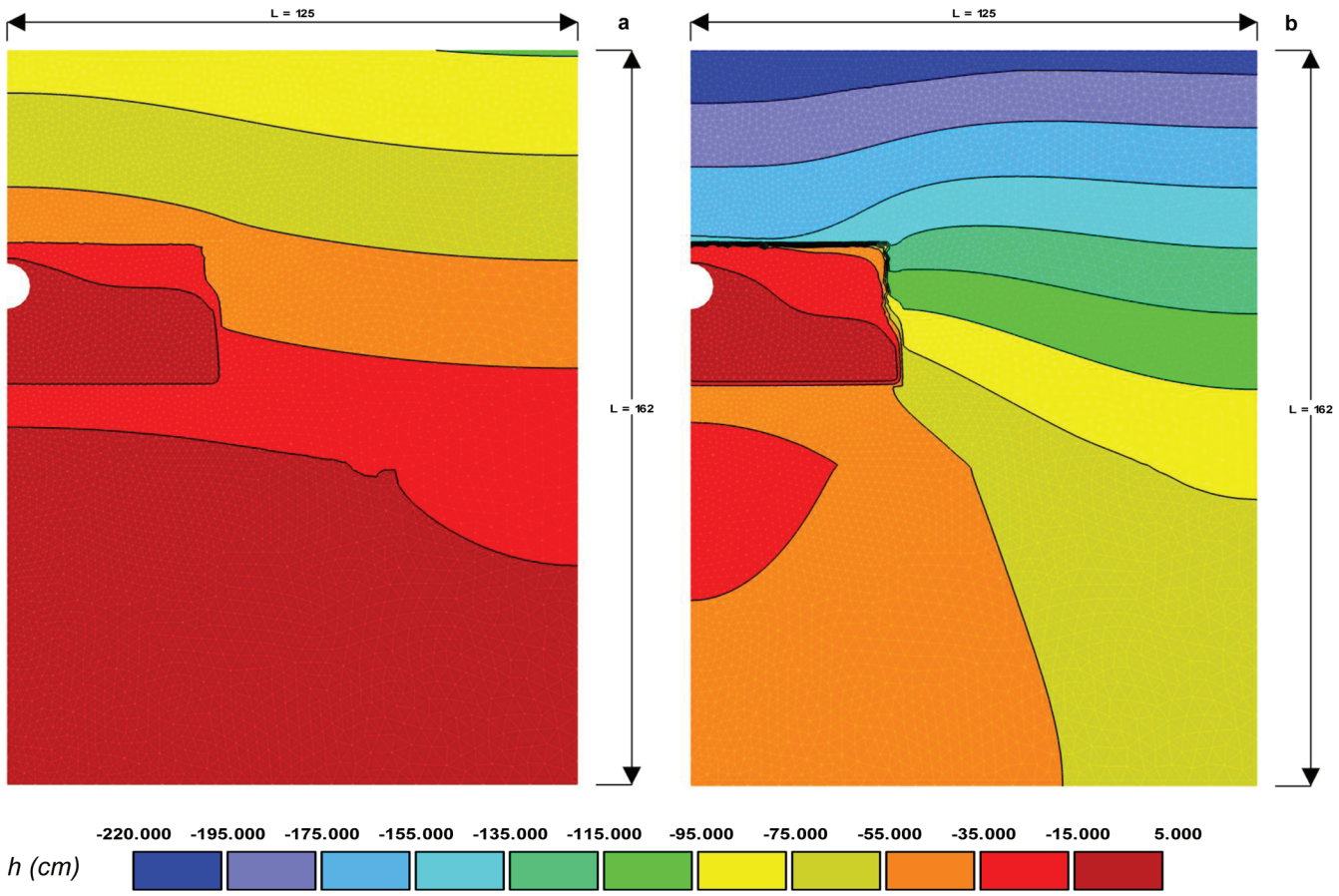

Fig. 4. Pressure head (h in cm) distribution in the drainfield during a wet [(a): 5088 h—29 Oct. 2009] and a dry [(b): 12960 h—22 Sep. 2010] period in the drainfield average simulation.

dosing malfunctions at the field site to capture the changes in pressure heads during periods where the dosing was slowed or stopped.

It is interesting to note that even during the longest period when the dosing apparatus was not working, measured pressure heads did not fall below −200 cm. During shorter periods when there was a malfunction, pressure heads did not fall below −100 cm. As such, the field capacity pressure head in this layered clay soil is certainly not −500 cm, as commonly assumed for a uniform clay soil (Romano and Santini, 2002). Instead it is slightly above the range (−100 to −400 cm) suggested by Twarakavi et al. (2009) for uniform clays. The reason for the high pressure head at field capacity is the low-K_s BC horizon which reduces percolation and acts like a water table at a shallow depth through most of the drainfield. Twarakavi et al. (2009) suggested that field capacity for layered soils may differ substantially from uniform soils.

The drainfield average simulated pressure head contours during a wet (29 Oct. 2009) and a dry (22 Sep. 2010) period are shown in Fig. 4. During the wet period (Fig. 4a), the soil was at or near saturation (h = −15–5 cm) directly below the trench bottom and denitrification would be favored with adequate NO_3^- and C availability under these conditions. It was also apparent that water ponded in the trench during the wet period. The soil above the trench was unsaturated during the wet period; however, small increases in water inputs from dosing or precipitation could cause the trench to completely fill with water and saturate the soil above the trench. During the dry period (Fig. 4b), pressure heads near the trench bottom and side walls ranged from −135 to −15 cm. There was a wet zone during the dry period directly beneath the trench bottom near the interface between the Bt and BC horizons (h = −15–5 cm) where K_s decreased from 0.945 to 0.145 cm h^{-1} (Table 1). Negative pressure heads near the trench-soil-interface indicated that the soil was unsaturated directly below the trench bottoms. Unsaturated conditions would be favorable for nitrification of NH_4^+ infiltrating into the trench bottoms. Saturated conditions at deeper depths in the drainfield would favor denitrification and nitrate would be expected to be available due to nitrification in the unsaturated zone directly below the trench bottom; however, C could be limiting at deeper depths. Low K_s values associated with the clay textured soil potentially increased water retention times in the soil. Slower water movement in the drainfield along with

Table 2. Calibrated HYDRUS solute transport parameters.

Material	ρ_b	Disp. L	Disp. T	K_d			Nitrification rate	Denitrification rate
				Cl^-	NH_4^+	NO_3^-	λ	μ
	g cm^{-3}	cm		L kg^{-1}			h^{-1}	
A	1.56	15	0.5	0.25	10	0.25	0.045	0.01
Bt	1.59	15	0.5	0.25	10	0.25	0.045	0.01
Gravel	1.67	15	0.5	0.25	10	0.25	0.045	0.01
BC	1.63	15	0.5	0.45	10	0.45	0.045	0.001
Biomat	1.59	15	0.5	0.25	10	0.25	0.045	0.01

soil water conditions very near saturation, as evidenced by pressure heads near 0 cm near the trench bottoms, could have also increased the amount of denitrification in the drainfield.

Drainfield Average Simulations: |Solute Transport

Chloride is present in wastewater and can be used as a tracer. Calibrated adsorption coefficients for Cl^- ranged from 0.25 to 0.45 L kg^{-1} (Table 2). The calibrated values for longitudinal and transverse dispersivity were 15 cm and 5 cm for the five materials, respectively (Table 2). Overall, the model fit between the observed and simulated Cl^- concentrations in the drainfield was good with RMSEs that ranged from 6.99 to 15.9 mg L^{-1} (Fig. 5). Simulated Cl^- concentrations at 15, 30, 60, and 90 U the trench bottoms typically resembled the mean observed concentrations in the drainfield. Variations in the Cl^- concentrations corresponded to variations in the monthly input concentrations at the variable flux boundary. Simulated Cl^- concentrations at 15, 30, 60, and 90 cm DS from the trench bottoms were higher than the observed concentrations, and often exceeded the standard error of the mean observed Cl^- concentrations. The simulated Cl^- concentrations were higher than the observed concentrations at the DS observation nodes because the model space assumed homogeneity within horizons whereas the soil horizons at the Griffin, GA OWTS site were more heterogeneous and actual K_d and dispersivities may have been more variable.

After 17,760 h of simulation, the Cl^- plume was well established in the drainfield (Fig. 6). The contours indicated that Cl^- was relatively evenly distributed below the trench bottom and concentrations ranged from 40 to 55 mg L^{-1} at the bottom of the model space. The highest Cl^- concentrations were away from the trench on this date because the monthly input concentration had decreased in the last month. The even distribution of Cl^- indicated that the wastewater plume had moved through most of drainfield profile after 17,760 h.

Our model simulated nitrification and denitrification as a function of water content (i.e., a surrogate for oxygen availability) in the drainfield. The water content dependency functions ($f_{sw,nit}$ and

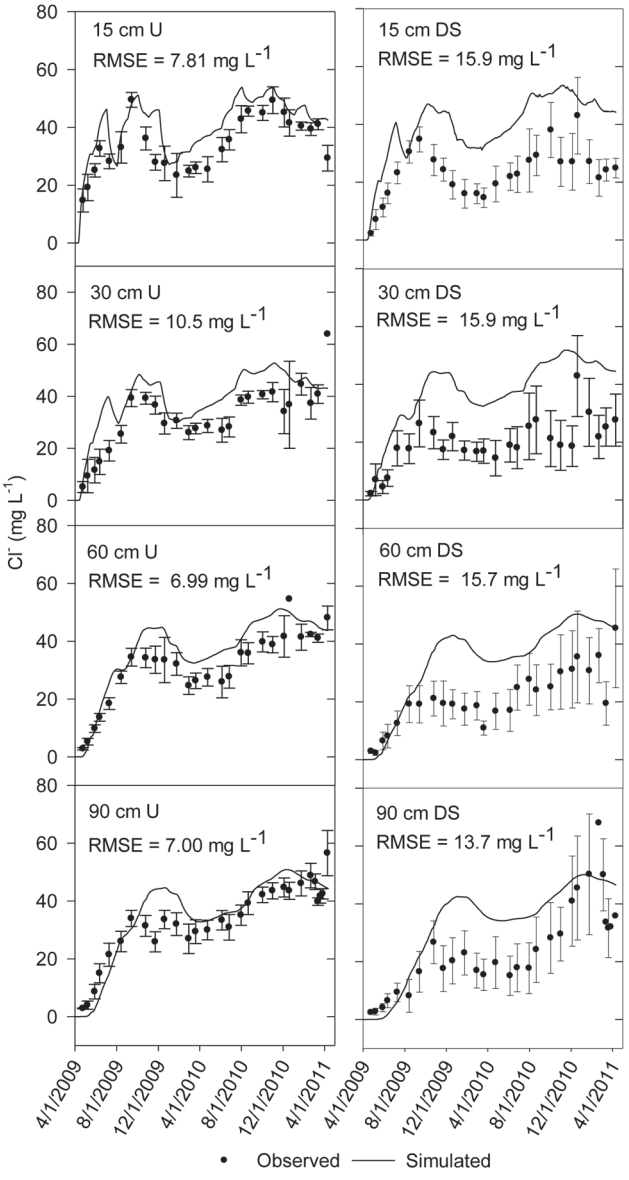

Fig. 5. Average observed drainfield Cl^- compared to simulated Cl^- concentrations at 15-, 30-, 60-, and 90-cm under (U) and downslope (DS) from trench bottoms, respectively in the drainfield average simulation. Error bars are standard error of the mean.

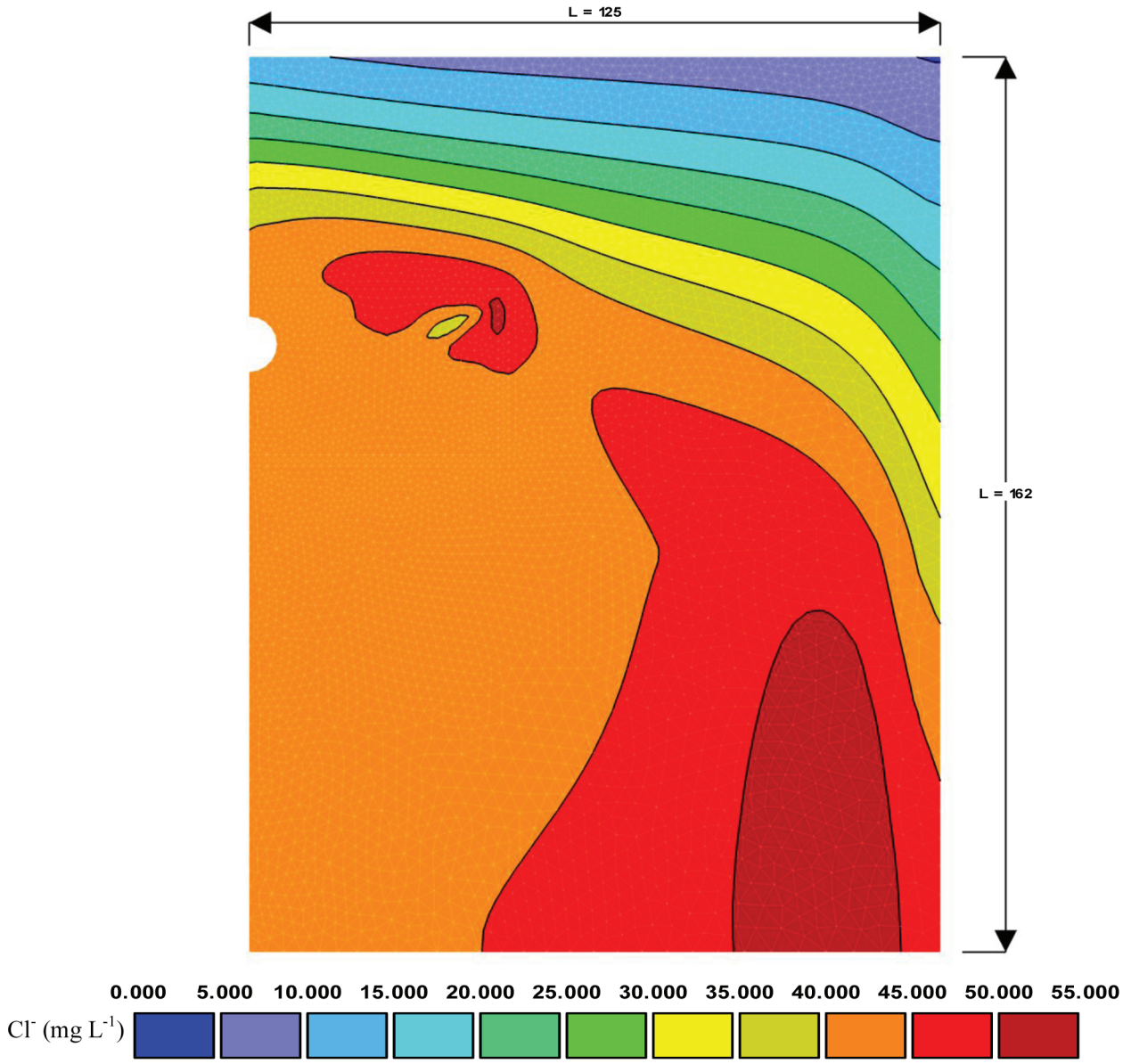

Fig. 6. Distribution of Cl^- in the drainfield after 17,760 h in the average simulation. The average Cl^- concentration of the septic tank effluent (STE) was 43.4 mg L^{-1}.

$f_{sw,denit}$ in Eq. [15]–[16]) are shown in Fig. 7 as a function of the absolute value of pressure head in the range from $h = 0$ to −1000 cm and as a function of relative water content (θ/θ_s). The soil water retention parameters for the Bt horizon (which were the same as those for the BC horizon and biomat) were used to convert water contents to pressure heads (Table 1). Water content dependent rate coefficients were calculated using Eq. [15]–[16] and parameter values were adjusted during calibration ($s_h = 0.94$, $s_l = 0.3$, $s_{wp} = 0.10$, $s_{dn} = 0.60$, $f_s = 0$, $f_{wp} = 0$, $e1 = 1$, $e2 = 2$, and $e3 = 1$) to achieve the best fit to the average NH_4^+ and NO_3^- concentrations with depth using the drainfield average, wet, and dry data subsets. Our pressure head data from the field study (Fig. 3) indicated that the soil did not become excessively dry during the study period and the modeled relative water content never dropped below 0.76, which is sufficiently high for nitrification to take place (Stark and Firestone, 1995). Our nitrification function differed from the function used by Beggs et al. (2011) in that the pressure head where nitrification rates began to decrease was much closer to saturation (Fig. 7). The reason why nitrification was not affected at near saturated conditions may be due to the fact that the trench was open to the atmosphere via the septic tank to the septic system vent (as are all OWTS) and this provided a supply of oxygen whenever the trench was not full of water.

On the wet end of the spectrum, the calibrated nitrification function began to decline when the pressure head rose above −50 cm

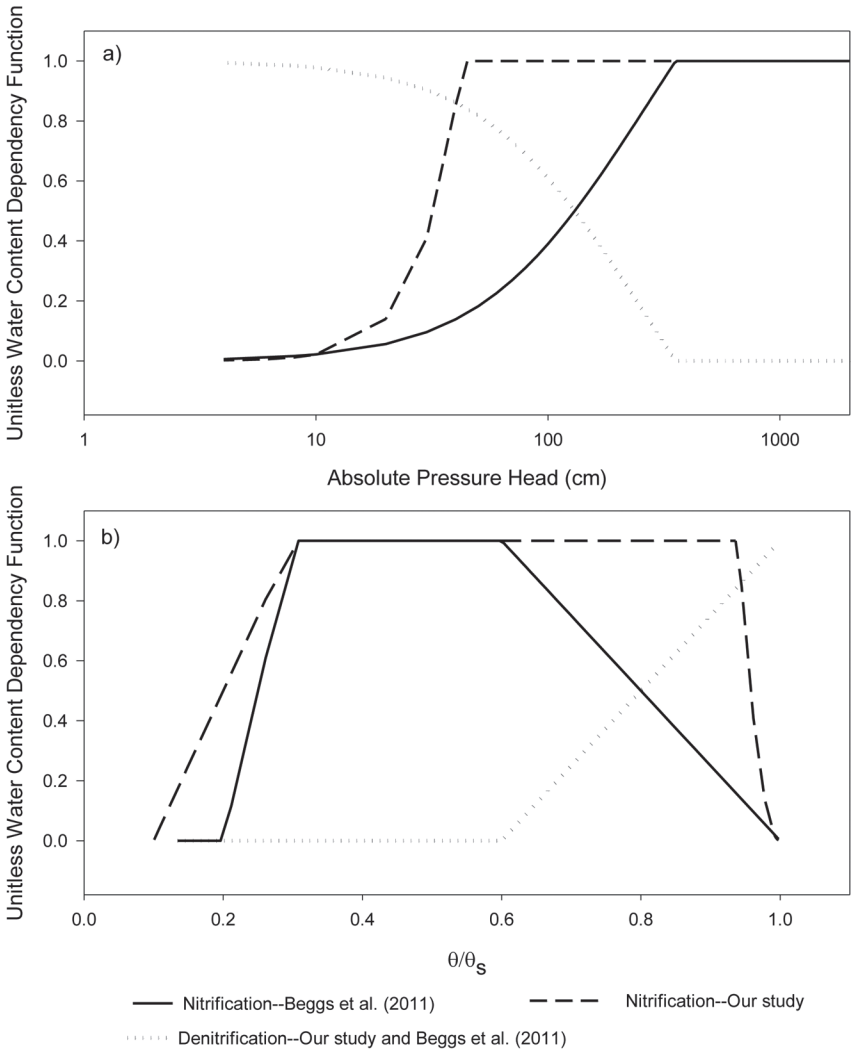

Fig. 7. Water content dependency functions for nitrification and denitrification vs. the absolute value of pressure head (a) and θ/θ_s (b) for our study and for Beggs et al. (2011).

and decreased to 0% of the maximum nitrification rate at saturation. On the dry end of the spectrum (not shown in Fig. 7), the function began to decrease at a relative water content of 0.30 and decreased to 0% at a relative water content of 0.10 (i.e., wilting point). For denitrification, the calibrated denitrification function was one at saturation and declined to zero at a pressure head of −360 cm (relative water content of 0.60). Our denitrification function was the same as that used by Beggs et al. (2011).

The model fit between the drainfield average predicted and measured NH_4^+ concentrations was good with RMSEs that ranged from 0.119 to 6.54 mg L^{-1} (Fig. 8). Simulated NH_4^+ concentrations were similar to measured NH_4^+ concentrations. The NH_4^+ concentrations were greatest at 15 cm under the trench bottom and decreased with depth and distance downslope. The NH_4^+ decreased in the drainfield due to adsorption and nitrification. The calibrated adsorption coefficient was 10 L kg^{-1} for all of the model layers (Table 2). We assumed that there was adsorption in the gravel because the aggregates were coated by a biofilm after 3 mo of wastewater dosing, as evident by visual identification of an organic layer on the trench bottoms through observation ports installed in the middle of each trench. The calibrated K_d was in the range of K_f values measured in the field (8.62–12.1 $L^{3\beta}$ $kg^{-\beta}$ where β is the Freundlich exponent), suggesting that most of the adsorption sites were occupied by NH_4^+. The calibrated first-order maximal nitrification rate was 0.045 h^{-1} for the five materials. This value was within the range of nitrification rates reported by McCray et al. (2005) and Pang et al. (2006). Most adsorption and nitrification occurred from 15 to 30 cm U and very little NH_4^+ was transported downward beyond the 30-cm U position (Fig. 8). A small amount of NH_4^+ was transported to the 15-cm DS position, as evidenced by low NH_4^+ concentrations at 15 cm DS. Very little NH_4^+ was transported beyond 15 cm DS as evidenced by low concentrations at 60 and 90 cm DS in Fig. 8. Like Cl^-, some

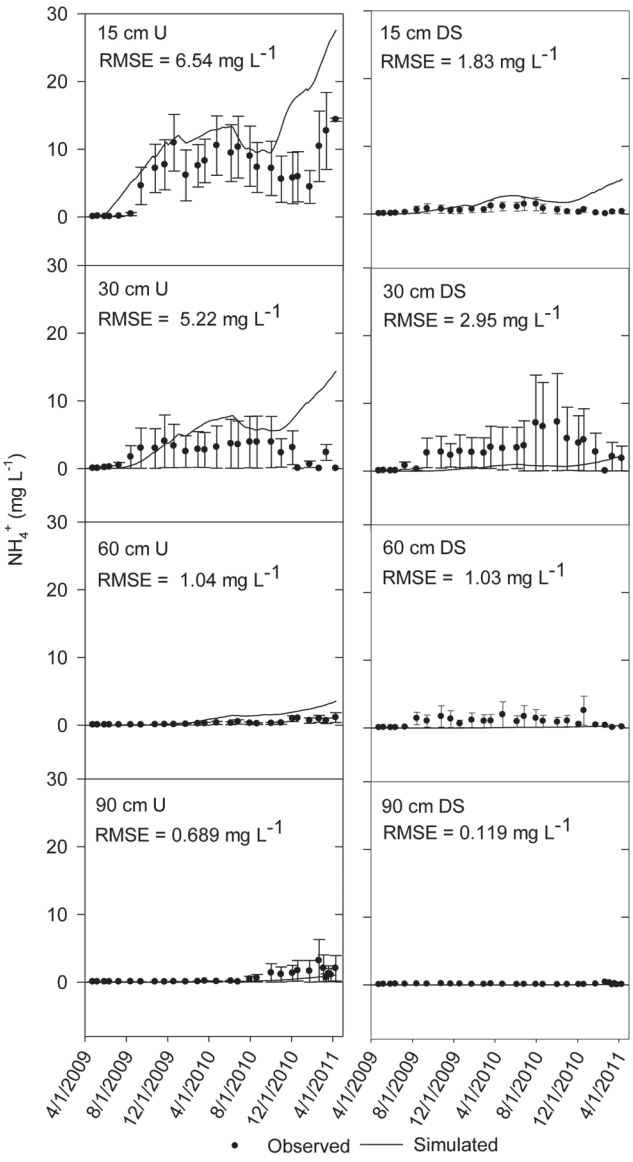

Fig. 8. Average observed drainfield NH_4^+ compared to simulated NH_4^+ concentrations at 15, 30, 60, and 90 cm under (U) and downslope (DS) from trench bottoms, respectively, in the drainfield average simulation. Error bars are standard error of the mean.

variation in NH_4^+ concentrations was due to variations in the input N concentrations. The input N concentration was high in September 2010 and January 2011, which probably increased the NH_4^+ concentration at 15 cm under the trench bottoms near the end of the simulation. The model captured seasonal variations in NH_4^+ concentrations due to differences in temperature and soil moisture content. The NH_4^+ concentrations tended to be greater in the winter months when nitrification was inhibited by lower temperatures and higher water content, and lower in the summer months when conditions for nitrification were more favorable due to higher temperatures and lower water content.

After 17,760 h of simulation, the NH_4^+ plume remained relatively close to the trench bottom (Fig. 9). The NH_4^+ concentration was greatest in the trench near the inlet pipe and decreased rapidly in the soil. As stated above, adsorption and nitrification were active in the region near the trench bottom and NH_4^+ was not very mobile in the drainfield. At steady state, the amount of NH_4^+ adsorbed to the soil would be in equilibrium with the concentration of NH_4^+ in solution. Higher input NH_4^+ concentrations would cause more NH_4^+ to be adsorbed and there would also be a higher concentration in solution. The higher solution concentration of NH_4^+ would undergo nitrification and NO_3^- concentrations would increase in the drainfield. Lower input N concentrations would cause NH_4^+ to desorb and nitrification would occur. Since the nitrification rate was first-order, the amount NO_3^- produced would depend on the NH_4^+ concentration. This will be discussed further below.

The fit between the drainfield average predicted and measured NO_3^- concentrations was adequate with RMSE that ranged from 4.86 to 8.10 mg L^{-1} (Fig. 10). Simulated NO_3^- concentrations were variable, but were similar to mean measured NO_3^- concentrations. Initially, the simulated NO_3^- concentrations at 15, 30, and 60 cm under the trench bottoms were higher than the observed concentrations. After November 2009, the simulated NO_3^- concentrations reached a steady state and were comparable to the observed concentrations. Adsorption probably slowed the NO_3^- plume and concentrations increased once the soil and soil solution reached steady state. Simulated and predicted NO_3^- concentrations were similar DS from the trench bottoms during most of the simulation period. The calibrated adsorption coefficients for NO_3^- were the same as those used for Cl^- (Table 2). The model captured seasonal variations in NO_3^- concentrations due to differences in temperature and soil moisture content. Simulated NO_3^- concentrations tended to be higher in the summer months when nitrification rates were high due to warmer temperatures and lower water content, and lower in the winter months when nitrification was inhibited due to cooler temperatures and higher water content.

After 17,760 h of simulation, the NO_3^- plume was well established in the drainfield (Fig. 11). The NO_3^- concentrations ranged from 0 to 30 mg L^{-1} in and directly below the trench. The NO_3^- concentrations were high just above the trench after 17,760 h, which was probably due to effluent drawn upward in the profile during periods when the trench was full, such as after a large rainfall. The NO_3^- concentrations increased with depth and decreased with distance from the trench. In addition, NO_3^- concentrations were not distributed as far in the drainfield as Cl^- concentrations because of denitrification. The NO_3^- concentrations also decreased from 30 to 25 mg L^{-1} near the bottom of the BC horizon due to denitrification. The calibrated maximal first-order denitrification rate for the A horizon, Bt horizon, biomat, and gravel was 0.01 h^{-1}, and for the BC horizon it was 0.001 h^{-1} (Table 2). The lower rate in the BC horizon was characteristic of a carbon-limited zone. These values

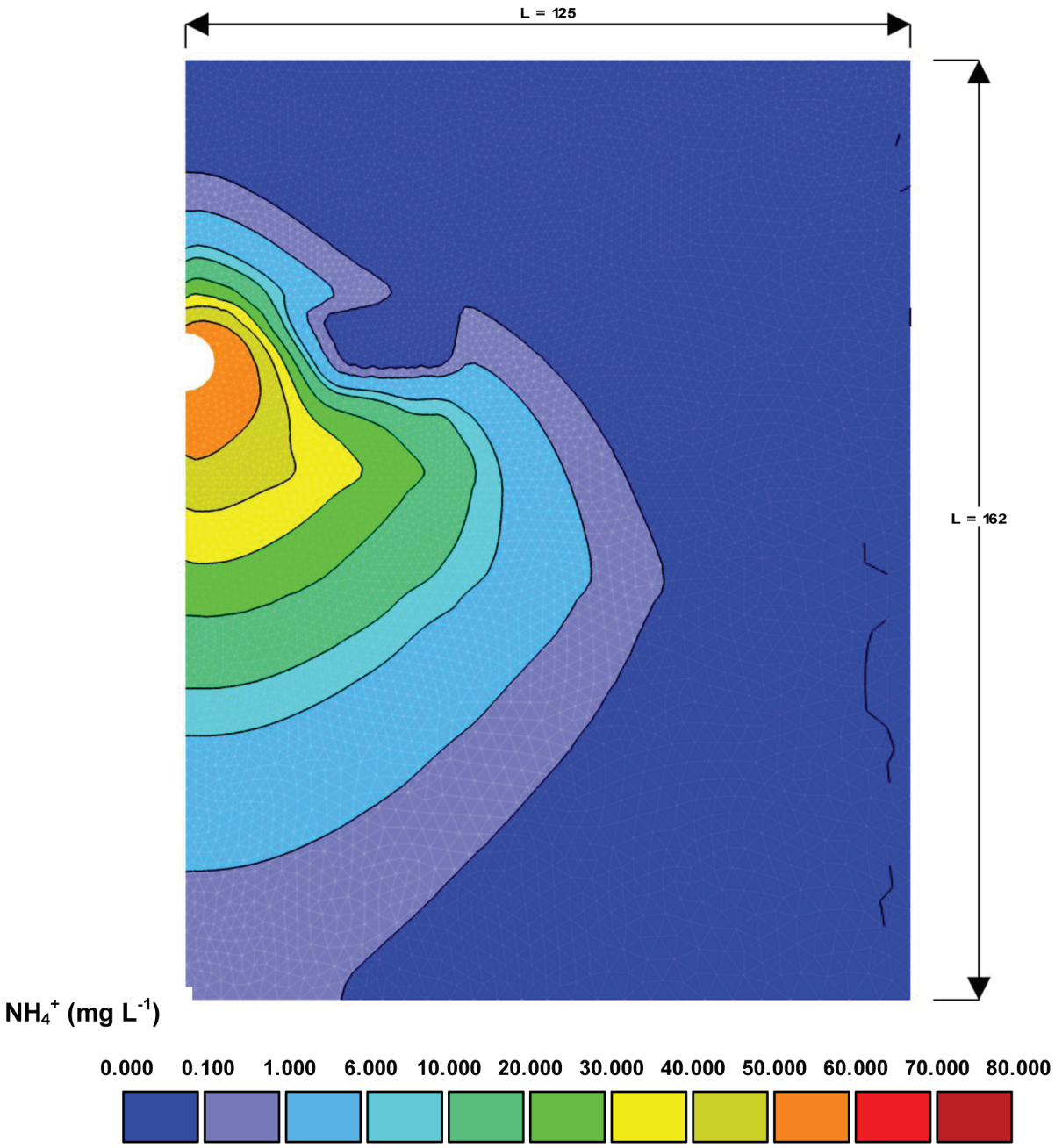

Fig. 9. Distribution of NH_4^+ in the drainfield after 17,760 h in the drainfield average simulation.

were within the range of first-order denitrification rates reported by McCray et al. (2005).

Wet End and Dry End Simulations

Wet- and dry-end simulations were evaluated using NH_4^+ and NO_3^- data collected from 3.3 m and 6.6 m from trench inlets, respectively. The fit between the predicted and measured NH_4^+ concentrations for the wet end simulation are shown in Fig. 12. In general, the model underestimated average NH_4^+ concentrations at the wet end of the trenches; however, the model fit was adequate with RMSEs that ranged from 0.183 to 6.43 mg L^{-1} for NH_4^+. The predicted NH_4^+ concentrations followed a seasonal trend, similar to the NH_4^+ concentrations in the drainfield average model run. Like the drainfield average simulation, NH_4^+ concentrations tended to be higher in the winter months when nitrification was inhibited by lower temperatures and higher water content, and lower in the summer months when nitrification was more favorable due to higher temperatures and lower water content.

The fit between the predicted and measured NO_3^- concentrations for the wet end simulation was good with RMSEs that ranged from 5.52 to 9.65 mg L^{-1} (Fig. 13). Initially, the simulated

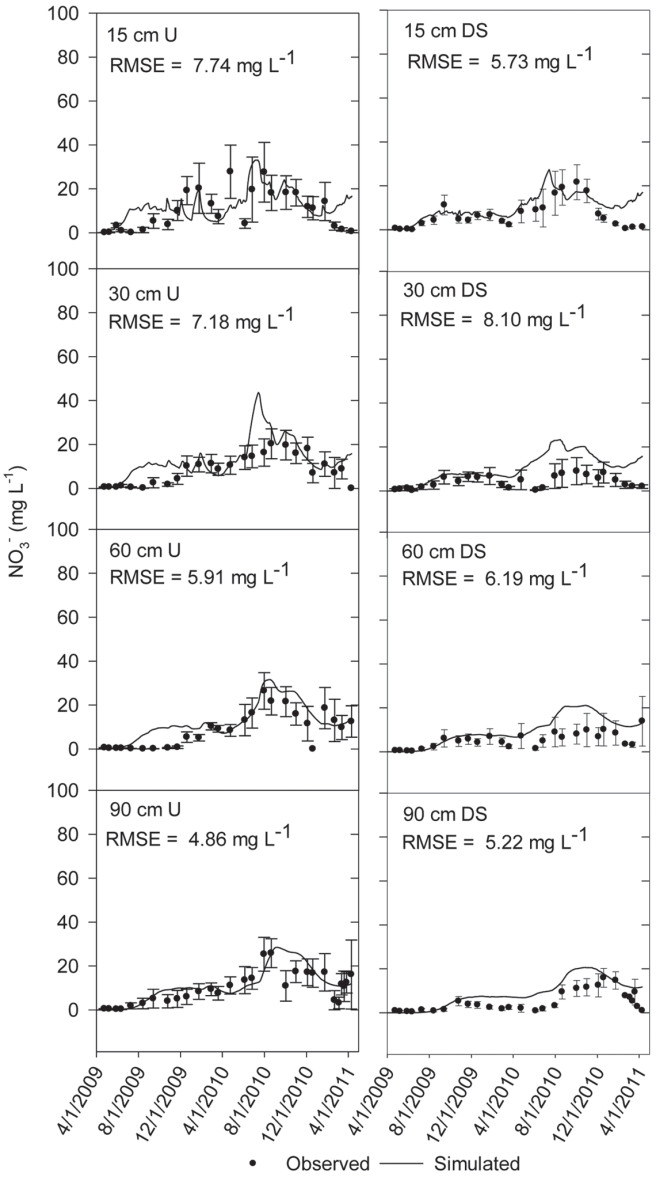

Fig. 10. Average observed drainfield NO_3^- compared to simulated NO_3^- concentrations at 15, 30, 60, and 90 cm under (U) and downslope (DS) from trench bottoms, respectively, in the drainfield average simulation. Error bars are standard error of the mean.

NO_3^- concentrations under the trench bottoms were higher than the observed concentrations. This indicated that the model overestimated the amount of nitrification or overestimated adsorption during the period when the system was newly installed and NO_3^- concentrations were still increasing in the soil solution. After approximately 1 yr of simulation (April 2010), the NO_3^- concentrations were similar to mean measured NO_3^- concentrations, which indicated that NO_3^- concentrations were probably at a steady state for the system. Like the drainfield average simulation, the wet end model also captured seasonal variations in NO_3^- concentrations with concentrations that tended to be higher in the summer months and lower in the winter months.

The fit between the predicted and measured NH_4^+ concentrations for the dry end simulation are shown in Fig. 14. The overall model fit was good with RMSEs that ranged from 0.0332 to 7.68 mg L^{-1}; however, the model over estimated NH_4^+ concentrations at 15 cm U and 30 cm U. Simulated NH_4^+ concentrations were lower in the dry end simulation than in the wet end simulation and reflected the smaller effluent dose that reached the dry end. Overall NH_4^+ concentrations were very low in the dry end of the drainfield which could have indicated the lower effluent dose along with rapid nitrification due to more aerobic (i.e., drier) conditions. This is supported by higher NH_4^+ concentrations at 30 cm U in the wet end simulation, because more effluent was applied and the nitrification rate was inhibited by the higher water content. There was a noticeable seasonal trend in NH_4^+ concentrations at the 15-cm U position, similar to the average and wet end simulations.

The fit between the predicted and measured NO_3^- concentrations for the dry end simulation was adequate with RMSEs that ranged from 4.89 to 10.6 mg L^{-1} (Fig. 15). Similar to the average simulation, the predicted NO_3^- concentrations under the trench bottoms were higher than the observed concentrations for the first few months and reached a steady state thereafter. Like the other two simulations, the dry end model also captured seasonal variations in NO_3^- concentrations with concentrations that tended to be higher in the summer months and lower in the winter months. The predicted NO_3^- concentrations in the DS positions were higher than the observed NO_3^- concentrations in the latter half of the simulation. This indicated that the nitrification rate was too high, the wastewater input was too high, or the denitrification rate was too low.

Temperature and Water Content Dependence: Drainfield Average Simulation

The differences between the predicted N concentrations in the wet and dry end simulations clearly highlighted the importance of including water content and temperature dependence on solute transport reactions. To further illustrate the effect of water content and temperature dependence on solute transport, we ran the optimized drainfield average simulation with WC only, with temperature (TEMP) only, and with no WC and no TEMP dependence, and compared the simulated nitrification and denitrification rates over time (Fig. 16) to the WC and TEMP dependent drainfield average simulation. Initially, all of the reaction rates increased until there was a steady state (e.g., November 2009). The highest nitrification and denitrification rates occurred when there was no WC and no TEMP dependence. Adding WC dependence and TEMP dependence individually decreased the reaction rates relative to the no WC and no TEMP. Combining WC and TEMP dependence had the greatest effect on reducing nitrification and denitrification rates. Since the denitrification rate curves were very similar to the nitrification rate curves, it appeared that denitrification was limited for the most part by the supply of NH_4^+.

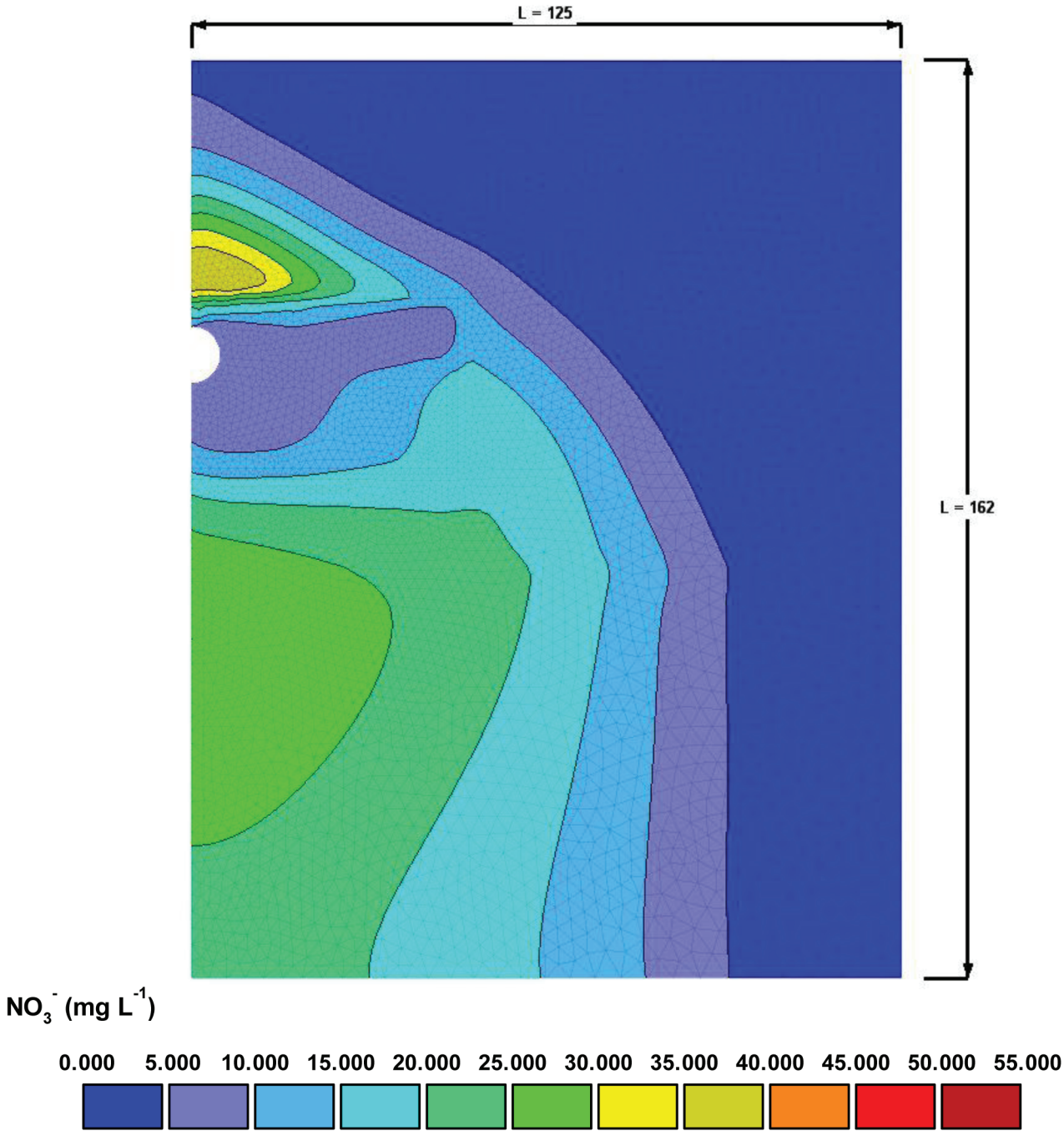

Fig. 11. Distribution of NO_3^- in the drainfield after 17,760 h in the drainfield average simulation.

Long Term Estimate of groundwater N loads

We measured N concentrations at the Griffin; however, we could not estimate an N load to groundwater because we did not know the water flux at the deepest depth. Models can provide accurate estimates of water flux across a boundary. We reran the calibrated average drainfield model for the same 2-yr cycle using the final pressure heads and N concentrations from the first run as initial conditions. By using the cumulative NO_3^- flux at the deep drainage boundary, we estimated N loads to groundwater for a mature OWTS where adsorption of N would not be an important sink because N concentrations were near steady state. The estimated leached N load for the experimental drainfield under long term conditions was 3.8 kg yr^{-1}. The final cumulative water flux from inputs (e.g., variable boundary flux and atmospheric flux) and outputs (e.g., root uptake flux and deep drainage flux) from the half-trench model space were converted to an average annual water flow for the drainfield (i.e., three 10-m-long trenches) and the mass water balance was calculated (Table 3). The total water yield from

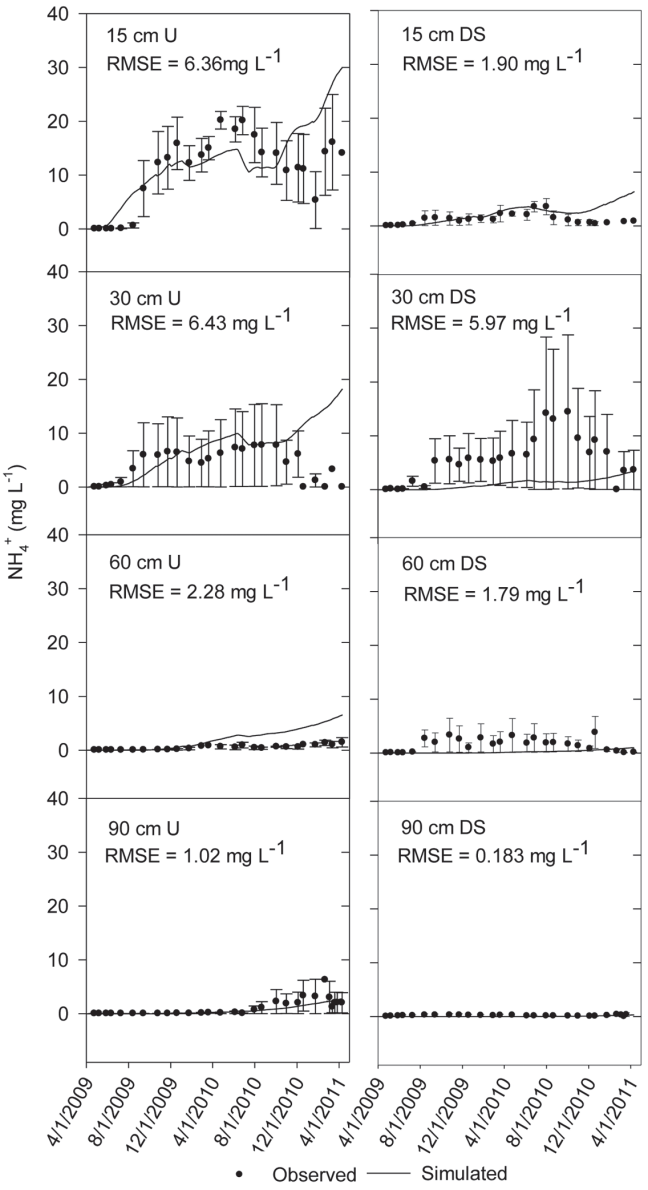

Fig. 12. Average observed NH_4^+ compared to simulated NH_4^+ concentrations at 15, 30, 60, and 90 cm under (U) and downslope (DS) from trench bottoms, respectively, in the wet end simulation. Error bars are standard error of the mean.

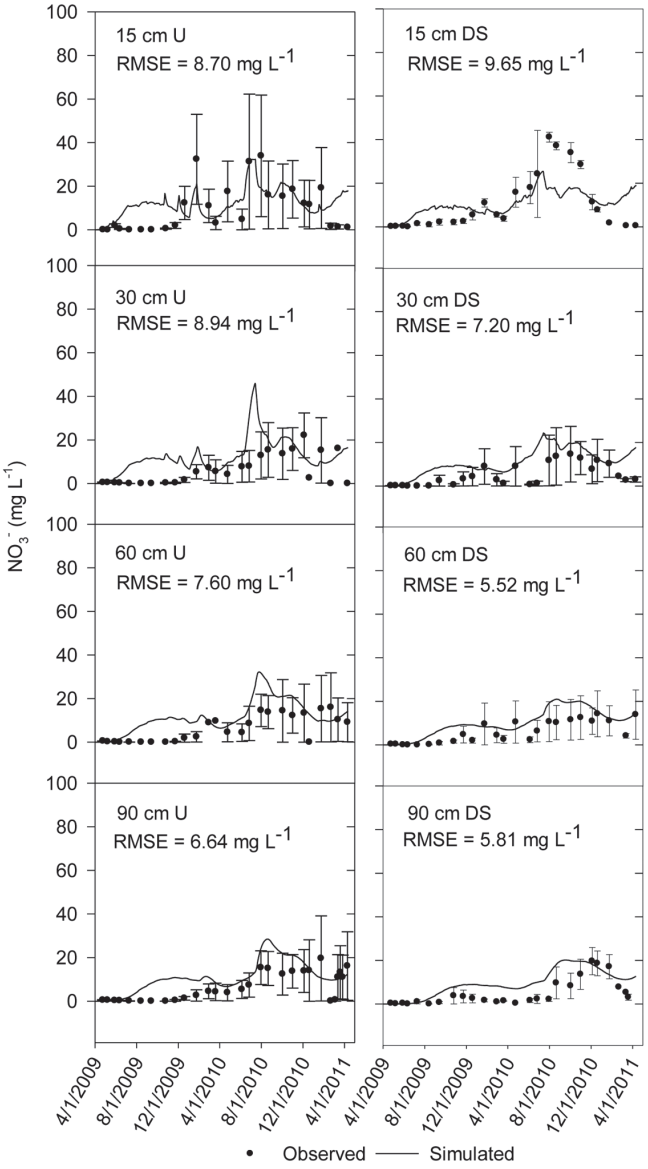

Fig. 13. Average observed NO_3^- compared to simulated NO_3^- concentrations at 15, 30, 60, and 90 cm under (U) and downslope (DS) from trench bottoms, respectively, in the wet end simulation. Error bars are standard error of the mean.

outputs (2.6×10^5 L yr^{-1}) were equal to total water inputs from wastewater dosing and precipitation.

Gold et al. (1990) measured nitrate concentrations below an OWTS drainfield, two lawns, a forest, and a corn field in Rhode Island. They used the CREAMS model (Smith and Williams, 1980) to estimate downward water flux. Samples were collected for 2 yr at all of the sites except for the OWTS drainfield which was monitored for 1 yr. They scaled up the OWTS load by assuming a zoning density of 5 homes ha^{-1} (1 home half-$acre^{-1}$). The annual nitrate load was 47.5 kg ha^{-1} for the OWTS site, 20.2–100.0 kg ha^{-1} for the corn sites, 1.3–9.3 kg ha^{-1} for the lawn sites, and 1.2–1.5 kg ha^{-1} in the forest site. Our Griffin OWTS drainfield was approximately 36% of a typical three-bedroom system (based on total waste applied) (GADCH, 2007; Radcliffe and West, 2009). Using our simulated long term N loads, the N load from a typical three-bedroom system in GA (e.g., 100 linear meters of drainfield) would be 11.5 kg yr^{-1}. Using a zoning density of 5 homes ha^{-1}, the N load would be 57.4 kg ha^{-1} yr^{-1}, which is quite close to the Rhode Island estimate. The OWTS load was also near the mid-range of loads estimated for agriculture (13 to 59 kg ha^{-1} yr^{-1}) by Havlin et al. (2005). As such, our estimated N groundwater load from high density OWTS represents a substantial input to groundwater.

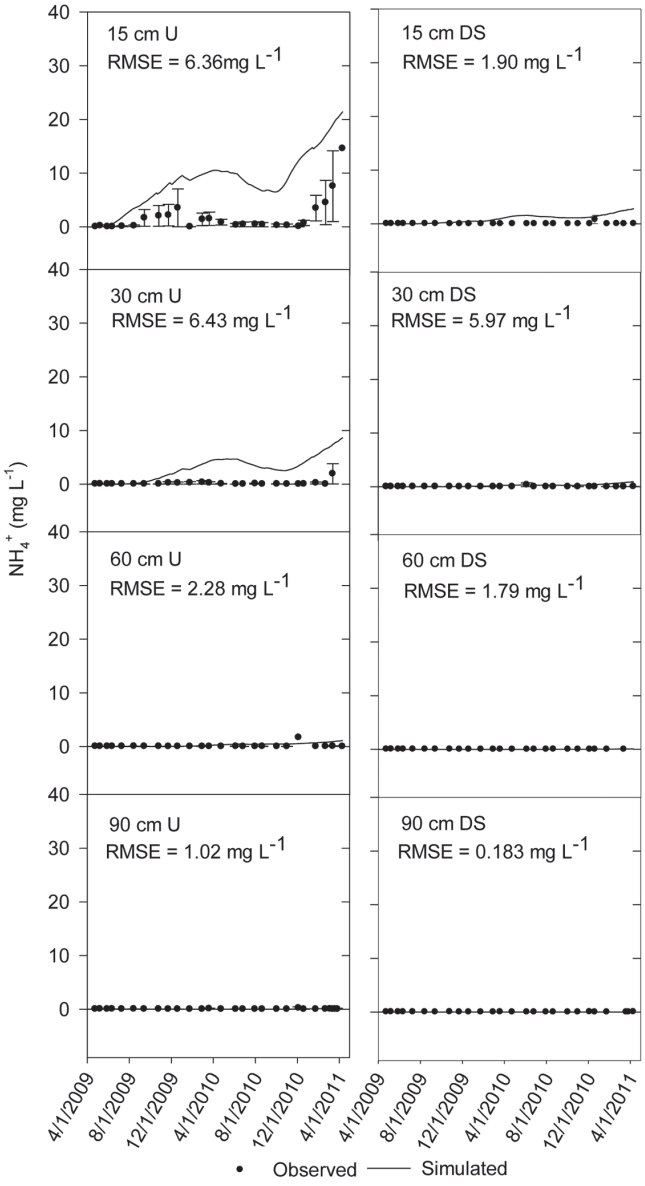

Fig. 14. Average observed NH_4^+ compared to simulated NH_4^+ concentrations at 15, 30, 60, and 90 cm under (U) and downslope (DS) from trench bottoms, respectively, in the dry end simulation. Error bars are standard error of the mean.

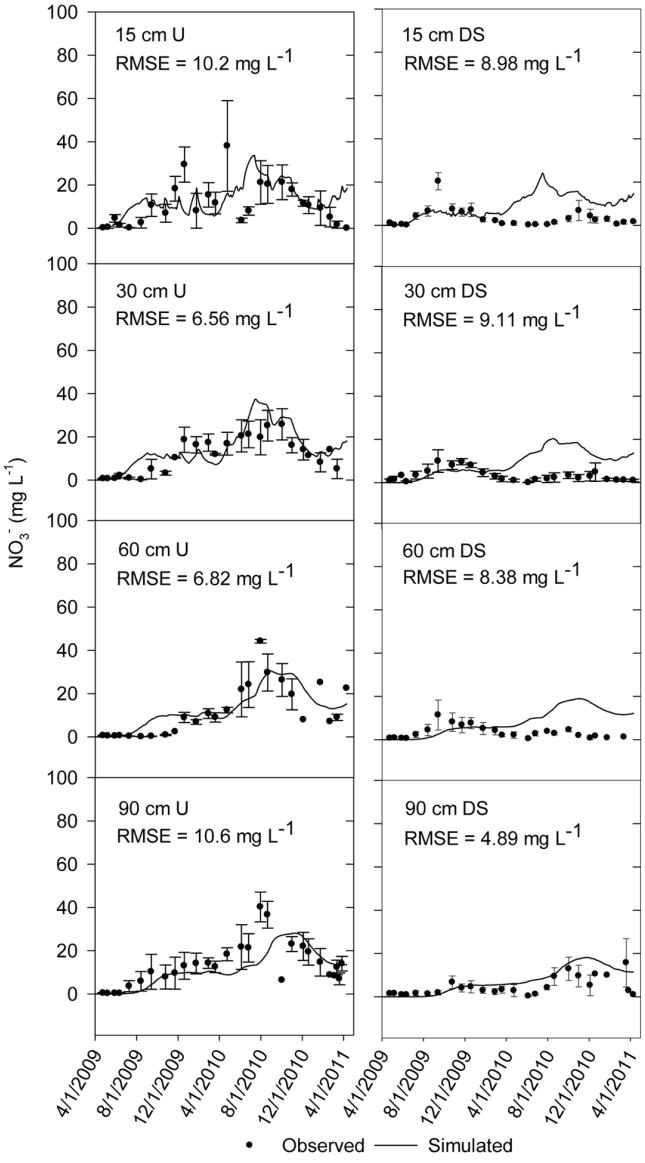

Fig. 15. Average observed NO_3^- compared to simulated NO_3^- concentrations at 15, 30, 60, and 90 cm under (U) and downslope (DS) from trench bottoms, respectively, in the dry end simulation. Error bars are standard error of the mean.

Estimate of Denitrification

The N mass balance based on the long term HYDRUS simulation was developed and expressed on an annual basis (Table 3). The input N load (9.7 kg yr^{-1}) was calculated from the cumulative flux of N dosed to the drainfield. The N lost to groundwater, calculated from the cumulative flux across the bottom boundary, was 3.8 kg yr^{-1}. The N loss from denitrification, calculated using the cumulative first-order transformation of NO_3^- to N_2, was 5.0 kg yr^{-1}. The total plant uptake of N, calculated from the cumulative uptake of NH_4^+ and NO_3^-, was 0.26 kg yr^{-1}. The N storage increased by 0.51 kg yr^{-1}, which accounted for changes in N adsorbed to the soil and N in solution in the drainfield.

The N mass balance was a steady state calculation of the overall N losses in a mature drainfield. Denitrification (52%) and leaching (39%) accounted for most of the N loss in the drainfield, while plant uptake (3%) and stored N (5%) were comparatively low. The denitrification estimated using steady state N:Cl ratios at the Griffin OWTS was 61% (Bradshaw and Radcliffe, 2013, this issue). The HYDRUS denitrification estimate was lower than what was estimated using the N:Cl ratios in the field because plant uptake was not accounted for with the N:Cl ratios and adsorption may

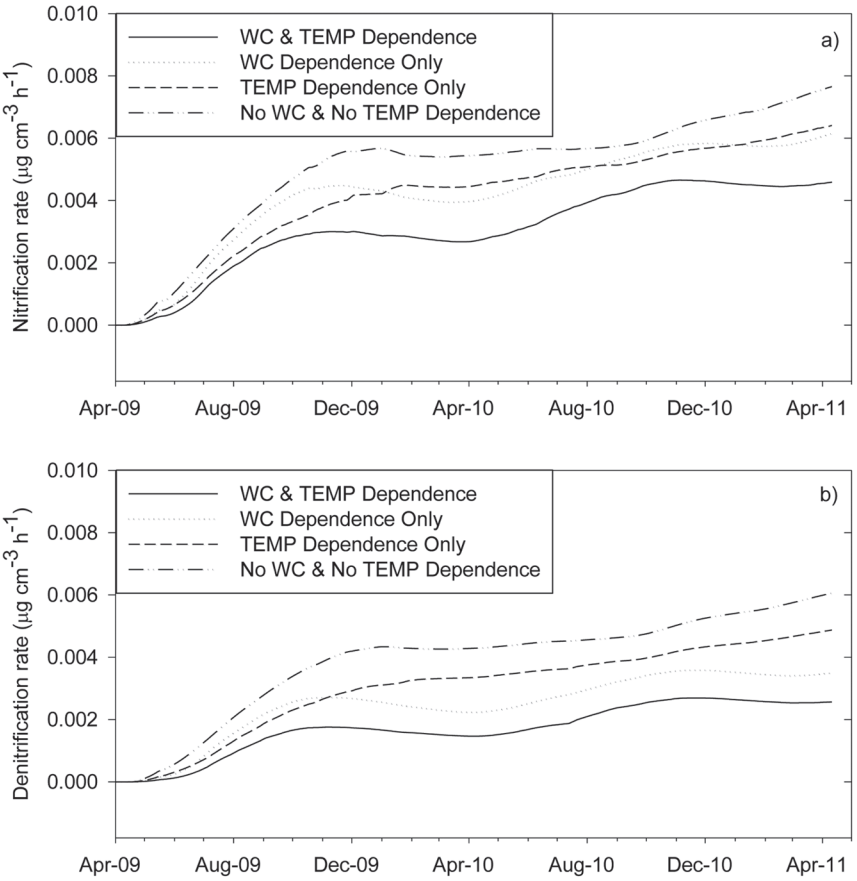

Fig. 16. Simulated nitrification (a) and denitrification (b) rates under different water content and temperature dependence scenarios in the drainfield average simulations.

Table 3. Mass balance of water and steady-state N in the drainfield.

Source	Water	% of input
	L yr^{-1}	
Effluent input	2.0×10^5	79%
Atmospheric input	5.4×10^4	21%
Total input	2.6×10^5	100%
Root uptake	6.2×10^4	24%
Deep drainage	1.9×10^5	76%
Total output	2.6×10^5	100%
Source	**N**	**% of input**
	kg yr^{-1}	
Input load	9.7	–
Leached	3.8	39%
Denitrification	5.0	52%
Plant uptake	0.26	3%
Storage	0.51	5%
Residual	0.18	2%
Total	–	100%

not have been at steady state (Bradshaw and Radcliffe, 2013, this issue). The HYDRUS estimate of denitrification represents the long-term estimate from a mature drainfield, and is similar to simulated denitrification estimates for fine-textured soils reported by Beggs et al. (2011).

Conclusions

Our study showed that the HYDRUS model was capable of simulating water movement and solute transport in an OWTS installed in a clay soil. Soil pressure heads were in a narrow range near saturation and the model fit was reasonable (RMSE of 37.4–35.8 cm). The calibrated solute transport parameters for adsorption and first-order N transformations were within the range of values reported in other studies (McCray et al., 2005; Pang et al., 2006). The drainfield average, wet end, and dry end simulations compared well to the solutes measured in the field [i.e., RMSE of 6.99–15.7 mg L^{-1} for Cl^- (average only), 0.0332–7.68 mg L^{-1} for NH_4^+, and 4.86–10.6 mg L^{-1} for NO_3^-].

Water and solute fluxes across the bottom boundary of the OWTS would have been difficult to measure in the field. The calibrated

model made it possible to estimate water and solute fluxes in the drainfield and N losses from the system. Based on the cumulative N flux from the steady state simulation, the estimated annual N losses from leaching at the lower boundary of the drainfield was 3.8 kg yr^{-1}. Scaled up to a typical OWTS size for GA and a zoning density of 5 homes ha^{-1}, the N load to groundwater (57.4 kg yr^{-1}) would be comparable to agricultural production losses to groundwater.

The model predicted denitrification accounted for 52% of the N removal in the system, while plant uptake and change in storage accounted for $\leq$5% of the N loss. These estimates should be valuable to TMDL developers who need to predict load allocations for nonpoint sources. These estimates were also specific to clay textured soils, which should be valuable for modeling N transport from OWTSs on a regional scale (i.e., Piedmont). In summary, the calibrated models accurately predicted OWTS water and N transport in the clay soil over a range of soil moisture conditions and the model may be extended to other soils found in the region.

Acknowledgments

This study was supported by a grant from the Water Environmental Research Foundation (proposal 36459-02) through the Colorado School of Mines, and funding from the Georgia Department of Public Health.

References

Beggs, R.A., D.J. Hills, G. Tchobanoglous, and J.W. Hopmans. 2011. Fate of nitrogen for subsurface drip dispersal of effluent from small wastewater systems. J. Contam. Hydrol. 126:19–28. doi:10.1016/j.jconhyd.2011.05.007

Beggs, R.A., G. Tchobanoglous, D. Hills, and R.W. Crites. 2004. Modeling subsurface drip application of onsite wastewater treatment system effluent. In K. Mankin, editor, Onsite Wastewater Treatment X: Proceedings of the Tenth National Symposium on Individual and Small Community Sewage Systems. Sacramento, CA. March 21–24, 2004. American Society of Agricultural Engineers, St. Joseph, MI. p. 92–103.

Bradshaw, J.K., and D.E. Radcliffe. 2013. Nitrogen fate and transport in a conventional onsite wastewater treatment system installed in a clay soil: Experimental results. Vadose Zone J. 12. doi:10.2136/vzj2012.0149 (this issue).

Brevé, M.E. 1994. Modeling the movement and fate of nitrogen in artificially drained soils. Ph.D. diss. North Carolina State University, Raleigh, NC.

Bumgarner, J.R., and J.E. McCray. 2007. Estimating biozone hydraulic conductivity in wastewater soil-infiltration systems using inverse numerical modeling. Water Res. 41:2349–2360. doi:10.1016/j.watres.2007.02.040

Crush, J.R., J.E. Walker, and D.A. Care. 2005. Root distribution and nitrate interception in eleven temperate forage grasses. Grass Forage Sci. 60:385–392. doi:10.1111/j.1365-2494.2005.00488.x

Feddes, R.A., P.J. Kowalik, and H. Zaradny. 1978. Simulation of field water use and crop yield. John Wiley & Sons, New York.

GADCH. 2007. Manual for onsite sewage management systems. http://health.state.ga.us/programs/envservices/landuse.asp (accessed 14 Jan. 2013).

GADNR. 2009. Draft total maximum daily load evaluation for two segments of Lake Allatoona in the Coosa River Basin for chlorophyll *a*. Georgia Department of Natural Resources, Atlanta, GA.

Gold, A.J., W.R. DeRagon, W.M. Sullivan, and J.L. Lemunyon. 1990. Nitrate-nitrogen losses to groundwater from rural and suburban land uses. J. Soil Water Conserv. 45:305–310.

Hassan, G., R.B. Reneau, Jr., and C. Hagedorn. 2008. Modeling effluent distribution and nitrate transport through an onsite wastewater system. J. Environ. Qual. 37:1937–1948. doi:10.2134/jeq2007.0512

Havlin, J.L., J.D. Beaton, S.L. Tisdale, and W.L. Nelson. 2005. Soil fertility and fertilizers. An introduction to nutrient management. 7th ed. Pearson Prentice Hall, Upper Saddle River, NJ.

McCray, J.E., S.L. Kirkland, R.L. Siegrist, and G.D. Thyne. 2005. Model parameters for simulating fate and transport of on-site wastewater nutrients. Ground Water 43:628–639. doi:10.1111/j.1745-6584.2005.0077.x

McCray, J.E., K. Lowe, M. Geza, J. Drewes, S. Roberts, A. Wunsch, D. Radcliffe, J. Amador, J. Atoyan, T. Boving, D. Kalen, and G. Loomis. 2009. State of the science: Review of quantitative tools to determine wastewater soil treatment unit performance. IWA Publishing, London.

NCDENR. 2001. Phase II total maximum daily load for total nitrogen to the Neuse River Esturary, North Carolina. NC Department of Enviroment and Natural Resources, Raleigh, NC.

Pang, L., C. Nokes, J. Šimůnek, H. Kikkert, and R. Hector. 2006. Modeling the impact of clustered septic tank systems on groundwater quality. Vadose Zone J. 5:599–609. doi:10.2136/vzj2005.0108

Radcliffe, D.E., and L.T. West. 2009. Design hydraulic loading rates for onsite wastewater systems. Vadose Zone J. 8:64–74. doi:10.2136/vzj2008.0045

Radcliffe, D.E., L.T. West, and J. Singer. 2005. Gravel effect on wastewater infiltration from septic system trenches. Soil Sci. Soc. Am. J. 69:1217–1224. doi:10.2136/sssaj2004.0302

Richards, L.A. 1931. Capillary conduction of liquids in porous mediums. Physics 1:318–333. doi:10.1063/1.1745010

Romano, N., and A. Santini. 2002. Field. In J.H. Dane and G.C. Topp, editors, Methods of soil analysis. Part 4 Physical methods. SSSA, Madison, WI. p. 721–738.

Schrader, L.E., D. Domska, P.E. Jung, Jr., and L.A. Peterson. 1972. Uptake and assimilation of ammonium-N and nitrate-N and their influence on the growth of corn (*Zea mays* L). Agron. J. 64:690–695. doi:10.2134/agronj1972.00021962006400050042x

Šimůnek, J., M.Th. Van Genuchten, and M. Šejna. 2008. Development and applications of the HYDRUS and STANMOD software packages and related code. Vadose Zone J. 7:587–600. doi:10.2136/vzj2007.0077

Smith, R.E., and J.R. Williams. 1980. Simulation of the surface water hydrology. In W.G. Knisel, editor, CREAMS: A field-scale model for chemicals, runoff, and erosion from agricultural management systems. Cons. Res. Rpt. No. 26. USDA, Washington, DC. p. 13–35.

Stark, J.M., and M.K. Firestone. 1995. Mechanisms for soil moisture effects on activity of nitrifying bacteria. Appl. Environ. Microbiol. 61:218–221.

Tchobanoglous, G, F.L. Burton, H.D. Stensel, and Metcalf and Eddy, Inc. 2004. Wastewater engineering, treatment and reuse. 4th ed. McGraw-Hill, New York.

Twarakavi, N.K.C., M. Sakai, and J. Šimůnek. 2009. An objective analysis of the dynamic nature of field capacity. Water Resour. Res. 45:W10410. doi:10.1029/2009WR007944

Twarakavi, N.K.C., J. Šimůnek, and M.G. Schaap. 2010. Can texture-based classification optimally classify soils with respect to soil hydraulics?. Water Resour. Res. 46: W02007. doi:10.1029/2009WR007939

USDA. 1996. Soil survey laboratory methods manual. Soil survey investigations report no. 42. National Soil Survery Center, Lincoln, NE.

USEPA. 2010. Guidance for federal land management in the Chesapeake Bay watershed. EPA Rep. 841-R-10–002. Office of Wetlands, Oceans, and Watershed. http://www.epa.gov/owow_keep/NPS/chesbay502/ (accessed 10 Nov. 2011).

van Genuchten, M.Th., F.J. Leij, and S.R. Yates. 1991. The RETC code for quantifying the hydraulic functions of unsaturated soils. Version 1.0. EPA Rep. 600/2–91/065. U.S. Salinity Laboratory, USDA, ARS, Riverside, CA.

van Genuchten, M.Th. 1980. A closed-form equation for predicting the hydraulic conductivity of unsaturated soils. Soil Sci. Soc. Am. J. 44:892–898. doi:10.2136/sssaj1980.03615995004400050002x

Walker, A. 1974. A simulation model for prediction of herbicide persistance. J. Environ. Qual. 3:396–401. doi:10.2134/jeq1974.00472425000300040021x

Youssef, M.A., R.W. Skaggs, G.M. Chescheir, and J.W. Gilliam. 2005. The nitrogen simulation model, DRAINMOD-N II. Trans. Am. Soc. Agric. Eng. 48:611–626.